Doctoral thesis

A novel pathway of DNA double-strand break formation that is independent of loop-axis tethering

Zhang Ying

August 2022

Laboratory of Genome and Chromosome Functions

Department of Biological Science

Graduate School of Science

Osaka University

TABLE OF CONTENT

List of Abbreviations

ATP	adenosine triphosphate
BSA	bovine serum albumin
CO	crossover
DAPI	6’-diamidino-2-phenylindole
DISS	dissection medium
DSB	double-strand break
DTT	dithiothreitol
EDTA	ethylenediaminetetraacetic acid
EtOH	ethanol
MI	meiosis I
MII	meiosis II
MIN	minimum medium
MES	2-(N-morpholino) ethane sulfonic acid
ml	milliliter
ORF	open reading frame
PAGE	polyacrylamide gel electrophoresis
PBS	phosphate-buffered saline
PCR	polymerase chain reaction
PFA	paraformaldehyde
RMM	Rec114-Mer2-Mei4 complex
SC/COM	synthetic complete medium
SD	synthetic dropout medium
SPS	sulphite polymyxin sulphadiazine
SPM	sporulation medium
TBS	Tris-buffered saline
TCA	trichloroacetic acid
TE	Tris-EDTA buffer
µl	microliter
YPAD	yeast peptone adenine D-glucose
YPG	yeast peptone glucose medium

Summary

Meiotic double-strand break (DSB) formation at early prophase I, which initiates homologous recombination, is essential for the meiosis. In budding yeast meiosis, Spo11, a topoisomerase VI-like protein, catalyzes DSB formation on chromatin loops. Spo11 induces DSBs by interacting with the RMM complex (Rec114–Mer2–Mei4) on the chromosome axis through loop-axis tethering, which is dependent of Spp1. Histone modification is essential for loop-axis tethering. PAF1C mediates histone H2BK123 ubiquitination, and Set1 then recognizes the ubiquitinated sites and subsequently methylates histone 3 lysine 4 (H3K4). Methylated H3K4 marks on chromatin loops are hotspots for DSB formation. Spp1 binds methylated H3K4 and tethers the hotspot to axis-bound Mer2, resulting in loops tethered to the axis. Then, Mer2 activates Spo11 to induce DSB formation. However, single *paf1c*, *set1,* or *spp1* mutants show a high level of DSBs, suggesting the presence of a loop-axis-tethering-independent regulatory pathway for DSB formation. In this thesis research, I found that the *paf1c* (*rtf1* and *cdc73)*, and *set1* mutants showed a synergistic decrease in the presence of a Myc-tag on either Rec114 or Mer2 in DSB formation. However, this DSB decrease was not induced in the *spp1,* a mutant in the most essential gene in the loop-axis tethering, with Myc-tag on RMM. Hence, in DSB formation, PAF1C and Set1 both play a role in meiotic DSB formation independent of the Spp1-mediated loop-axis tethering. I speculate that PAF1C and Set1 may collaboratively methylate a component of the DSB machinery and this collaboration is critical for DSB formation in the absence of loop-axis tethering.

Chapter I. Introduction

Meiosis is a specific cell cycle which provides haploid gametes from diploid germ stem cells. Defects in meiosis are responsible for primary sterility, miscarriage, and congenital disorders. Understanding molecular mechanisms of meiosis could guide future research that is applied for the diagnosis and clinical treatment of infertility related to meiotic defects, and improve the health of our offspring [1]. Homologous recombination is an essential step during meiosis in which a physical connection is formed between homologous chromosomes. Double-strand break (DSB) formation initiates reciprocal exchange of homologous chromosomes, crossover, a type of recombination. DSB formation is regulated by histone modification machinery as well as the subsequent loop-axis tethering. However, in the single mutants of critical genes involved in the histone modification machinery, the number of DSBs is only decreased to one-third level of wild-type. Importantly in the single mutant of loop-axis tethering machinery, the number of DSBs show a slight reduction instead of abolishing DSBs. These results suggest the presence of regulatory mechanisms, which is independent of histone modification and/or loop-axis tethering. In this thesis, I will describe a new regulatory mechanism that induces DSB formation independent of loop-axis tethering configuration through the histone modification machinery.

1. Budding Yeast

Budding yeast, *Saccharomyces cerevisiae*, is commonly known as baker`s yeast or brewer`s yeast. Budding yeast is a powerful tool used to analyze cell cycle control, chromosome functions, and other aspects of cell biology. If budding yeast is placed under the condition of sufficient nutrition, its cell cycle is rapidly completed from 90 min to 2 hr. The budding yeast gene has 15 million base pairs on 16 chromosomes, on which analyses can be performed easily within a relatively short time. Budding yeast proliferates by producing buds. The optimal temperature for budding yeast to survive is 30 °C. Budding yeast has two mating-type genes, *MATa* and *MATα*. The *MAT* locus is on the right arm of chromosome III and determines the cell type. Cells expressing type “a” secrete a-factor and bear the α-factor receptor, while α cells secrete α-factor and are detected by their expression of the a-factor receptor. Upon binding with mating

pheromones, haploid cells polarize toward fusion with the opposite mating type for the formation of a diploid cell. Cells with a mating projection are called “Shmoos”, which is a cartoon character with a shape similar to this projection. The diploid zygote has fused nuclei. Interestingly, the haploid form of budding yeast has the ability to switch to the other mating type; for instance, in this yeast, *MATa* can be exchanged with *HML* α or *MATα* can be exchanged with *HMR a*, and *HMR a* and *HML* α are called mating-type cassettes [2]. Similar to that in other eukaryotic species, the genetic information in budding yeast is also maintained mainly in chromosomes in the nucleus with some information maintained in mitochondria [3].

2. Meiosis

1-2-1. The meiotic cell cycles

Budding yeast undergo meiosis only when ‘pressured’ to do so, with meiotic entry governed by relative nutritional availability. When growth conditions are optimal, mitosis is the default division process since it enables rapid growth utilizing the available nutrients. However, in response to nitrogen starvation or lack of fermentable carbon sources, yeast diploid mitotic cells arrest at the G1 phase of mitosis and activates meiotic program to generate progeny [4]. Cells undergo two consecutive cycles of chromosome segregation: meiosis I and meiosis II. During meiosis I, homologous chromosomes are separated to opposite poles. After that, two daughter cells are generated. In meiosis II, sister chromatids pull apart toward opposite poles, resulting in the production of haploid gametes, four spores in the case of the budding yeast (Fig. I).

Meiotic prophase I

There are five stages in meiotic prophase: leptotene, zygotene, pachytene, diplotene stages, and diakinesis.

Leptotene stage:

In the leptotene stage, chromosomes appear as “thin threads”. Diffuse chromosomes condense into thin and long strands. After the formation of multiple chromatin loops with a chromosome axis, DSB formation is initiated and followed by the end processing;

meiotic recombination starts from this stage [5]. Rad51 and Dmc1, yeast homologs of RecA, the major bacterial strand exchange protein, which mediates repair of DSBs for crossover formation in inter-homolog recombination, are loaded on single-stranded DNAs (ssDNAs) of the DSB ends [6-9].

Zygotene stage:

During the transition from the leptotene to the zygotene stage, the telomeric ends of the chromosomes attach to the inner membrane of the nuclear envelope and are clustered in one area of the nuclear envelope. This structure looks like a flower cluster, inspiring scientists to call this transition stage the bouquet stage. After the formation and processing of DSB ends, the single-end invasion intermediate (SEI), which is invasion by one DSB end into a homologous duplex DNA is formed concomitantly with the onset of synaptonemal complex (SC) formation, a meiosis-specific chromosome structure formed between homologous chromosomes at early zygotene stage. SEI formation is completed during the period of SC formation [10]. SCs formed during meiotic prophase I are known to regulate DSB formation and to promote the preferential repair of DSBs in homologs over those in sister chromatids. In the zygotene stage, SC formation is partially completed with synapsis of some homologous regions [11].

Pachytene stage:

SCs are completely formed between homologous chromosomes all along axes in the pachytene stage [12]. In meiotic recombination, the double-Holliday junction (dHJ) intermediates form by the processing of the SEIs at early pachytene stage [13]. As the pachytene stage ends, the resolution of dHJs reveals the formation of crossovers [14]. The polo-like kinase of Cdc5 is implicated in disassembly of SCs and dHJ resolution as well as pachytene exit [15].

Diplotene stage:

The SC breaks down in this stage. The homologous chromosomes are highly agglutinated, and the chiasma, which often shows the X-shaped chromosomal structure, is visible at the sites of crossover between homologous chromosomes at this stage.

Diakinesis:
The chromosomes are condensed more than diplotene stage. During the end of diakinesis, spindle fibers start to form and prepare for homologous chromosome separation in meiosis I.

Meiosis I and Meiosis II:
In meiosis I, homologous chromosomes move in a bioriented fashion with the force by spindles. Crossing-over provides a physical basis for the tension on mono-polar kinetochores by spindles. Meiosis I is completed when the homologous chromosomes separate. The number of chromosomes is reduced by one-half in each daughter cell, but each kinetochore of the homologous chromosomes has a pair of attached sister chromatids for mono-polar attachment. In meiosis II, after the dissolution of mono-polar kinetochores, the sister chromatids separate as tension forms in the sister spindles [16, 17], eventually producing four gametes with a haploid set of 16 chromosomes in each budding yeast cell (Fig. I).

1-2-2. Meiotic recombination

Homologous recombination in meiosis is crucial in chromosome segregation during meiosis by providing a physical linkage between homologous chromosomes, known as chiasma, which creates one tension on the separation of homologous chromosomes. By the formation of crossover with exchanging genetic information between homologous chromosomes, a new combination parental alleles is generated (Fig. II).

Meiotic homologous recombination starts with DSB formation. The 5'-end resection generates a long 3' tail of ssDNA, and invades the homologous DNA strand [18]. With searching of homologous DNAs and strand exchange, a displacement loop (D-loop) structure is formed, which corresponds with SEI. Further DNA synthesis by the DNA synthesis enzyme drives D-loop extending to form a dHJ intermediate and ultimately resolves into crossovers. (Fig. III).

Rad51 and Dmc1: Rad51 is a strand exchange protein that forms a helical filament with ssDNAs and searches for homologous duplex DNAs. Rad51 is involved in the recombination repair of DSBs during mitosis and meiosis. Dmc1 is a meiosis-specific

homolog of Rad51. Although both Rad51 and Dmc1 are essential for DSBs repair in meiosis, Rad51 does not participate directly in strand exchange between homologous chromosomes but facilitates Dmc1-mediated DNA strand exchange [19]. These proteins are often used as a marker for the presence of DSB with ssDNAs as well as DSB repair/recombination.

3. Histone modification affects the formation of meiotic DSBs

Spo11 is an evolutionarily conserved topoisomerase VI-like enzyme that generates DSBs in meiotic early prophase I. DSBs are non-randomly distributed along chromosomes [20]. In budding yeast, there are ten DSB formation factors in three interaction groups: Spo11-Ski8-Rec102-Rec104, which is Spo11 complex; Rec114-Mei4-Mer2, which is RMM complex; and Mre11-Rad50-Xrs2, which is MRX complex [21]. DSB formation is associated with histone methylation, such as H3K4 mono-, di- and trimethylation, as well as H3K79 trimethylation. In budding yeast, the Set1 complex (Set1C or COMPASS) catalyzes all H3K4 methylation, in which Set1 not only catalyzed the methylation, but also serves as a scaffold for seven subunits (Bre2, Sdc1, Shg1, Spp1, Swd1, Swd2, and Swd3). Set1 mediates COMPASS complex stability and all H3K4 methylations while Spp1 is important, not for methylation of H3K4, but for reading H3K4me3 by PHD domain [22, 23].

1-3-1. Histone modification

Histone modifications are key epigenetic regulatory features that have important roles in many cellular events. Histone posttranslational modification (PTM) includes phosphorylation, methylation, ubiquitination, acetylation, SUMOylation, and others which are involved in signaling and remodeling at the DSB [24]. The nucleosome is the basic chromatin packing unit, and 146 bp of DNA wraps the surface of the nucleosome in 1.7 turns. The nucleosome contains a histone octamer, two H3-H4 dimers, and two H2A-H2B dimers. In the nucleosome octamer, the outward-extending N-terminal tails are sites of regulatory modification [25, 26]. Modifications of all four histones have been reported, but those affecting H3 and H4 are best understood [27-29]. Histone modifications are correlated with gene expression, transcription activation, and influences the repair of damaged DNA [30].

Ubiquitination

Ubiquitin is a small regulatory protein of 76 amino acids with 2 α-helices and β-sheets. Ubiquitination of target proteins is realized through the actions of a series of specific enzymes that leads to the specific modification of the targeted proteins. Proteins are marked by ubiquitin in three steps. In the first step, the activating protein (E1) binds to ubiquitin and transfers this ubiquitin to an E2 conjugate protein, which is the ubiquitin carrier. In the second step, the E2 protein combines with E3 ligase protein, and the E3 protein recognizes and ubiquitinates the target protein by linking the ubiquitin to the target protein to mark it for the change of functions such as targeted degradation. In 1975, H2A was characterized as the first ubiquitinated protein in eukaryotes. Since then, ubiquitination has been discovered for all four core histones, the histone variants H2A.X and H2A.Z, and the linker histone H1 in many organisms [31]. Mono-ubiquitination of H2B contributes to gene silencing and transcription activation. H2A ubiquitination is important for transcriptional repression in higher eukaryotes [32]. Histone ubiquitination also plays a role in replication [33], transcription, and the DNA damage response [34]. The ubiquitination of H2B also serves as a marker for the methylation of histone H3.

Histone methylation

Methylation of histones makes nucleosomes pack tightly together. Histone methylation regulates chromatin structure and functions depending on the modified residues and the number of methyl groups. Methylation status of histones is regulated by histone methyltransferases and demethylases. There are more than sixty kinds of histone methyltransferases and demethylases have been identified. Histone methylation occurs on the tail at arginine 2 and lysine 4, 9, 27, 36, and 79 of histone H3. Histone arginine residues can be mono- or di-methylated, and histone lysine residues can be mono-, di-, or tri-methylated [35]. Methyltransferase Set1 mediates H3K4 methylation for transcription activation [36] and DSB formation at promoters during meiosis [37]. H3K9, which is critical for heterochromatin formation in most eukaryotes, does not undergo methylation in budding yeast [38]. H3K27 methylation is associated with gene expression [39]. Set2 mediates H3K36 methylation and regulates diverse activities, including DNA repair, mRNA splicing, and suppression of inappropriate transcription during transcription elongation [40]. Dot1 is the sole H3K79 methyltransferase that

mediates H3K79 methylation for transcriptional regulation, cell cycle regulation, and the DNA damage response [41].

1-3-2. Hotspots and cold spots of DSB formation

Meiotic recombination preferentially starts in a specific region called the recombination hotspot. The first discovered DSB was associated with a hotspot of recombination at the *ARG4* locus of budding yeast. The hotspots are nonrandomly distributed along chromosomes and do not contain any specific DNA sequence in most organisms including budding yeast [42]. In the yeast, there are three types of hotspots: α hotspots whose activity is dependent on transcription factor binding, β hotspots with intrinsically open intergenic DNA sequences, and ɣ hotspots with high GC levels [43]. Most DSB hotspots are preferentially located in promoter regions in *S. cerevisiae* [44]. Indeed, in the budding yeast, most of the DSB hotspots localize at the NDR (nucleosome-depleted region). Furthermore, DSB hotspots are located in chromatin loops rather than chromosome axes. These suggest the dynamic regulation of DSB formation by chromatin structure or sub-structures during meiosis. There are several methods for mapping where Spo11 acts and sequencing of Spo11-associated oligonucleotides (Spo11 oligos) is the most accurate till 2022, specifying the locations of DNA breaks to the base pair [45].

Telomeres, centromeres, and mating-type loci are cold genomic regions for DSB formation. The centromere of chromosome III locally represses both crossing over and gene conversion, thus DSB formation [43].

1-3-3. Meiotic DSB formation

DSB formation is restricted to a narrow window of time in meiosis to ensure the proper execution of the recombination function and prevention of toxic DNA lesion production at improper times [46]. DSB formation starts in the leptotene stage in meiosis, and its repair is completed in the pachytene stage with the formation of the synaptonemal complex, which represses DSB formation.

Spo11: Spo11, Rec102-Rec104, and Ski8 form a complex to produce DSBs. Spo11 is similar as topoisomerase VI A subunit in archaea. Top VI consists of A and B subunits. The top VI A subunit catalyzes strand cleavage reaction, and B subunit is a regulatory subunit. Indeed, a recent study showed that Spo11 and Ski8 were A

subunits of Top VI and that Rec102-Rec104 form a complex that was similar with the B subunit of Top VI (Fig. IV, left). To break double-stranded DNA, the active-site tyrosine 135 in Spo11 dimer catalyzes dual nucleophilic attacks on the phospho-diester bonds of the both DNA strands. These trans-esterification reactions result in covalent Spo11-oligoDNA complexes, with Spo11 monomer attaching to the 5' terminal end of both broken ends. After the removal of Spo11-oligoDNA by nicking and processing of the DSB ends, the ends extensively resect the 5' end strands to generate ssDNA for strand searching invasion. Most recombination events are initiated by a single Spo11-mediate DSB. Recently scientists uncovered a closely localized DSB, called double-DSB, separated by just ~33 to over 100 base pairs [47].

RMM: Rec114, Mei4, and Mer2, which are essential for DSB formation, form the complex of Rec114-Mei4-Mer2 (RMM). The RMM localizes to chromosome axes from leptotene stage. Although the localization of Rec114 and Mer2 to chromosomes are independent of each other, deletion of either leads to failure to generate DSBs [48]. Together or in some regions not with meiotic cohesin complex containing Rec8, meiosis-specific chromosome-axis proteins, Hop1 and Red1, recruit RMM to the chromosome axis and then RMM recruits Spo11 complex to form DSBs. Phosphorylation of Mer2 at Ser30 residue by Cdc7 and CDK in the S phase is not required for the localization of Mer2 but is essential for the assembly of Mei4 and Rec114 to the chromosome axis [49, 50] with partially overlapped localization on meiotic chromosome axes [48, 51, 52]. DSB formation may trigger Mer2 dephosphorylation, which in turn lead to its dissociation from chromosomes and its subsequent degradation [53].

DSB processing factors: Mre11, Rad50, and Xrs2 forms the MRX complex, which is essential to homologous recombination and nonhomologous end-joining during mitosis as well as DSB formation during meiosis in budding yeast. How the MRX contributes to DSB formation during meiosis remains to be solved. Xrs2 is essential for the nuclear localization of Mre11 [54]. In the DSB resection, MRX collaborates with Sae2 nuclease to release Spo11-complex from DSB ends [55, 56].

DSB formation and histone modification

In addition to the NDR region free for nucleosomes at promoters, DSB hotspots show unique features of histone modification such as histone H2BK123 ubiquitination, H3K4 methylation and H3K79 methylation, etc. in the budding yeast. This tight association of histone H3K4 methylation is also conserved in mammals including humans. The mutants deficient in the H3K4 methylation show reduced frequencies of DSBs.

To introduce the H3K4 methylation in the promoter regions of the genes, upon the initiation of the transcription, the RNA polymerase II associating complex, PAF1C, is recruited to the 5' region of the gene, which then activates the Rad6/Bre1 ubiquitin ligase E2/E3 complexes to ubiquitinate H2BK123. The ubiquitination mark promotes the recruitment of Set1C/COMPASS to mediate H3K4 methylation.

PAF1C: RNA polymerase II elongation complex (PAF1C) includes five subunits: Rtf1, Paf1, Cdc73, Ctr9, and Leo1 in budding yeast. PAF1C acts importantly not only in interacting with transcriptional factors, facilitating the chromatin templates elongation, recruiting the 3' processing factors for transcription termination but also in recruiting and activating histone modification factors [57]. Interestingly, as a general regulator for the production of mRNAs, the dysfunction of PAF1C is associated with Parkinson's disease, which is a neural cell disease that usually occurs in elderly men.

Among mutants in the five subunit genes of PAF1C, *ctr9* and *paf1* deletion mutants grow poorly in the vegetative phase and enter meiosis inefficiently and asynchronously, since both *CTR9* and *PAF1* are critical genes to regulate efficient transcription in the G1 phase. Leo1 is essential for the dynamic regulation of heterochromatin and therefore, it does not affect the methylation of H3K4 or H3K79 and thus is not essential for DSB formation [58]. Therefore, the Rtf1 and Cdc73 subunits, which are essential for facilitating Bre1/Rad6 in H2BK123 ubiquitination and subsequent H3K4 histone methylation, is a main interest for the analysis of PAFC subunits in meiotic DSB formation [59].

Rtf1: The main subunit of PAF1C, Rtf1, regulates gene expression by directing co-transcriptional histone modification (H2BK123 ubiquitination and H3K4 methylation). Because deletion of amino acids 62-109 or 112-152 prevents the ubiquitination of histone H2B, these combined regions are termed the histone modification domain (HMD) of Rtf1 [60]. Expression of the HMD is sufficient to restore global H2B K123 ubiquitination in a yeast strain in which endogenous *RTF1* has been deleted, and this

is a conserved region among species [61, 62].

Cdc73: Cell division cycle 73 (Cdc73) has a Ras-like C domain that constitutes a protein interaction surface that functions with Rtf1 in coupling PAF1C to the RNA polymerase II elongation machinery, but this Ras-like C domain is not required for PAF1C assembly [63]. In humans, *cdc73* causes hyperparathyroidism-jaw syndrome and parathyroid tumors.

Set1: Set1/COMPASS components include Set1, Spp1, Bre2, Sdc1, Swd1, Swd2, Swd3, and Shg1 [64]. Set1 is a histone methyltransferase that mediates the mono-, di- and tri-methylation of histone H3 lysine 4 after sensing ubiquitinated sites and ultimately contributes to DSB formation. Set1 contains a SET domain of 130 amino acids forming an active site that facilitates substrate binding and dictates product specificity [65]. Set1 mediates H3K4 methylation near promoters in both mitotic and meiotic cells, which is followed by DSB hotspot formation [66].

Spp1: Spp1 is the cardinal subunit of Set1/COMPASS. Spp1 primarily recognizes trimethylated histone. Spp1 also promotes efficient H3K4 methylation by the Set1 complex. The H3K4 is trimethylated at the 5’ end of active genes, and its adjacent arginine residue H3R2 is read by the PHD finger of Spp1 [36]. In meiosis, Spp1 can physically interact with both H3K4me3 and Mer2, located at the meiotic chromosomal axis [67].

1-3-4. Loop-axis tethering

Each chromatid is organized into a linear array of chromatin loops, comprising the bases of a structural axis, which is called the chromosome axis [12]. The meiosis-specific Rec8-cohesin provides physical basis of the axes with the loop, probably by loop-extrusion activities and promotes the association of meiosis-specific axis proteins. Red1 and Hop1, both of which are necessary for efficient DSB formation. As a complex of DSB formation factors, RMM is also located on the chromosome axis [48]. The Set1/COMPASS -independent role of the Spp1 protein involves translocation of Spp1 to the chromosome axis through interaction with Mer2. Spp1 has a PHD finger, reads H3K4me3 on the chromatin loop, and brings H3K4me3 regions to the chromosome axis [66, 68]. This recruitment of the hotspot to the chromosome axis is referred to as

“loop-axis tethering” (Fig. IV, right). This loop-axis tethering model is a widely accepted model for meiotic DSB formation.

4. Aim of my research

Histone modification, which plays a critical role in meiotic DSB formation, is highly regulated. Histone H3K4 methylation is catalyzed by the Set1C/COMPASS complex, in which Set1 directly catalyzes the methylation of histone H3K4. Histone H3K4 methylation depends on histone H2B K123 ubiquitination. Ubiquitination of this histone is catalyzed by the combined action of Rad6 and the Bre1, E2, and E3 ubiquitination enzymes, respectively. In addition, the RNA polymerase II-associating factor I complex PAF1C is essential for H2BK123 ubiquitination and thus H3K4 methylation (Fig. V). PAF1C consists of five subunits, Rtf1, Cdc73, Paf1, Leo1, and Ctr9. Previous studies have shown that mutations in genes involved in histone modification machinery are necessary for efficient DSB formation. H3K4-mediated loop-axis tethering seems to be critical for DSB formation. However, interestingly, all mutations in the *SET1*, *RTF1*, and especially *SPP1* genes involved in loop-axis tethering reduce the number of DSBs differentially but do not eliminate DSB formation. This suggests the presence of an additional regulatory pathway mechanism of DSB formation, which is independent of loop-axis tethering. In my thesis, to reveal a new regulatory pathway for meiotic DSB formation, I studied the genetic interaction between histone modification machinery and DSB machinery for meiotic DSB formation.

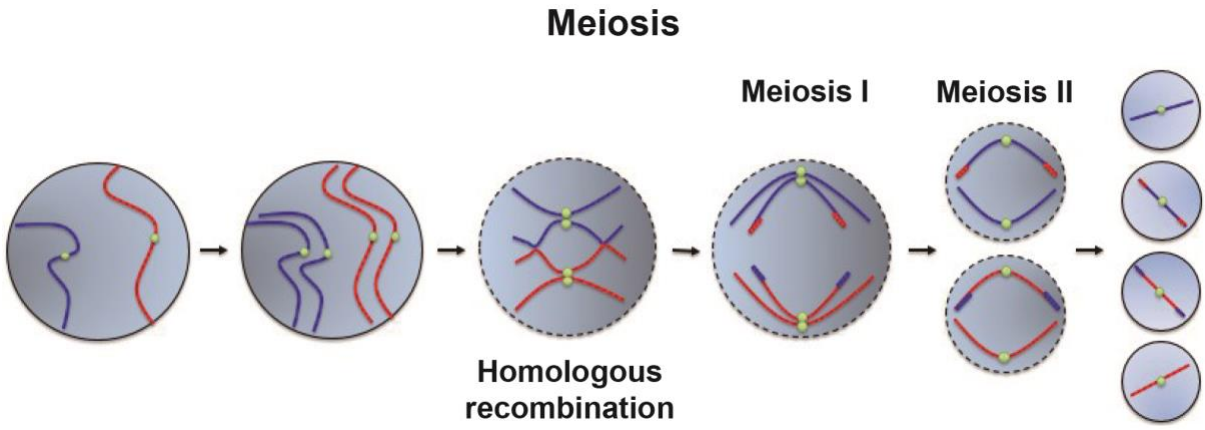

Fig. I Meiosis

Meiosis is a specialized cell division that produces haploid gametes from diploid germ cells. In meiosis I, homologous chromosomes align and then move to opposite poles. In Meiosis II, four haploid cells are produced upon sister chromatid separation.

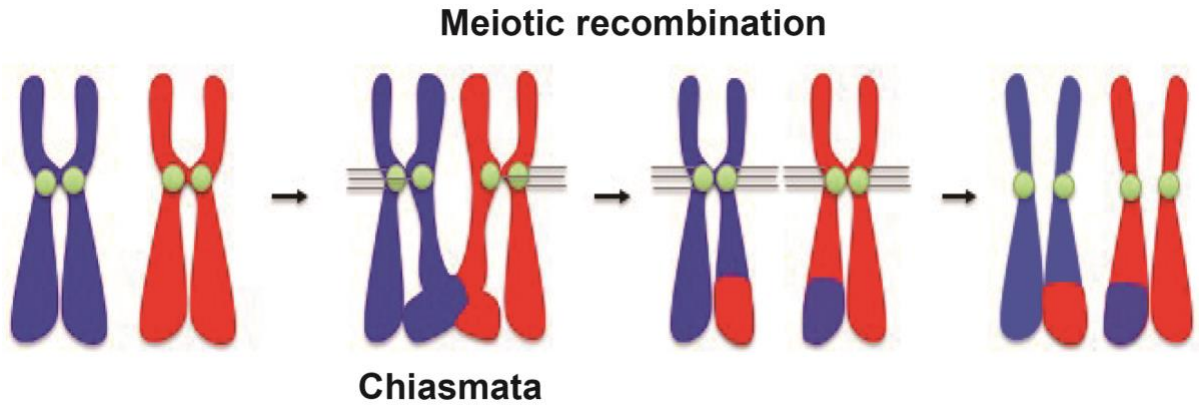

Fig. II Meiotic Recombination

Recombination follows the reciprocal exchange of homologous chromosomes, which provides a physical connection that promotes the segregation of chromosomes and the generation of new combinations of alleles.

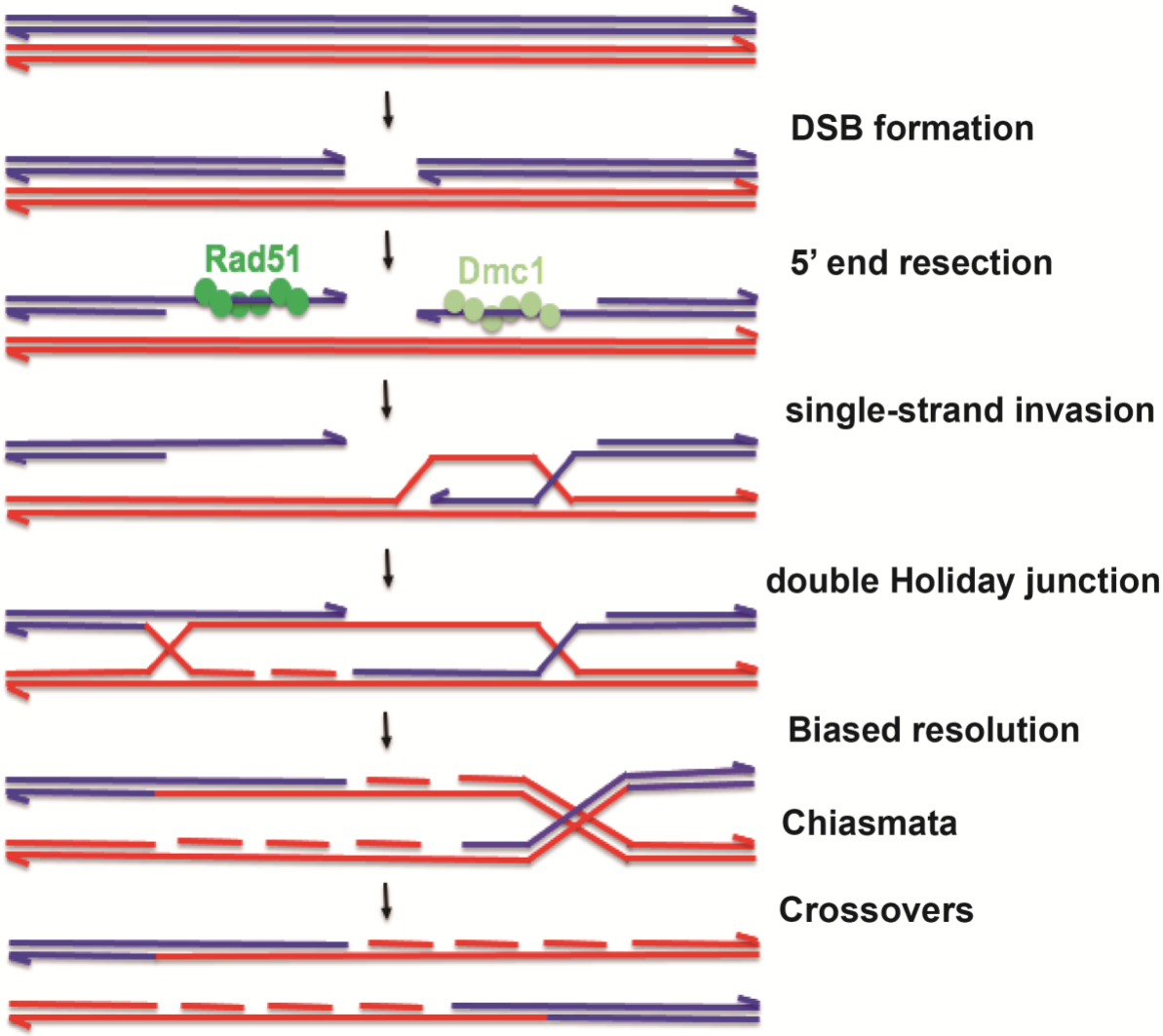

Fig. III Mechanism of Meiotic Recombination

Meiotic recombination is initiated upon the formation of DNA double-strand breaks (DSBs). DSBs are subject to 5’ end resection, resulting in single-stranded DNA (ssDNA). Recombinases such as RecA-like proteins Rad51 and Dmc1 bind to perform searching for the homologous strand and strand exchange between ssDNA and homologous duplex DNAs. Further DNA synthesis and processing results in the formation of a double Holliday junction and is finally biased resolved into crossover recombinants, which is a molecular basis for chiasma.

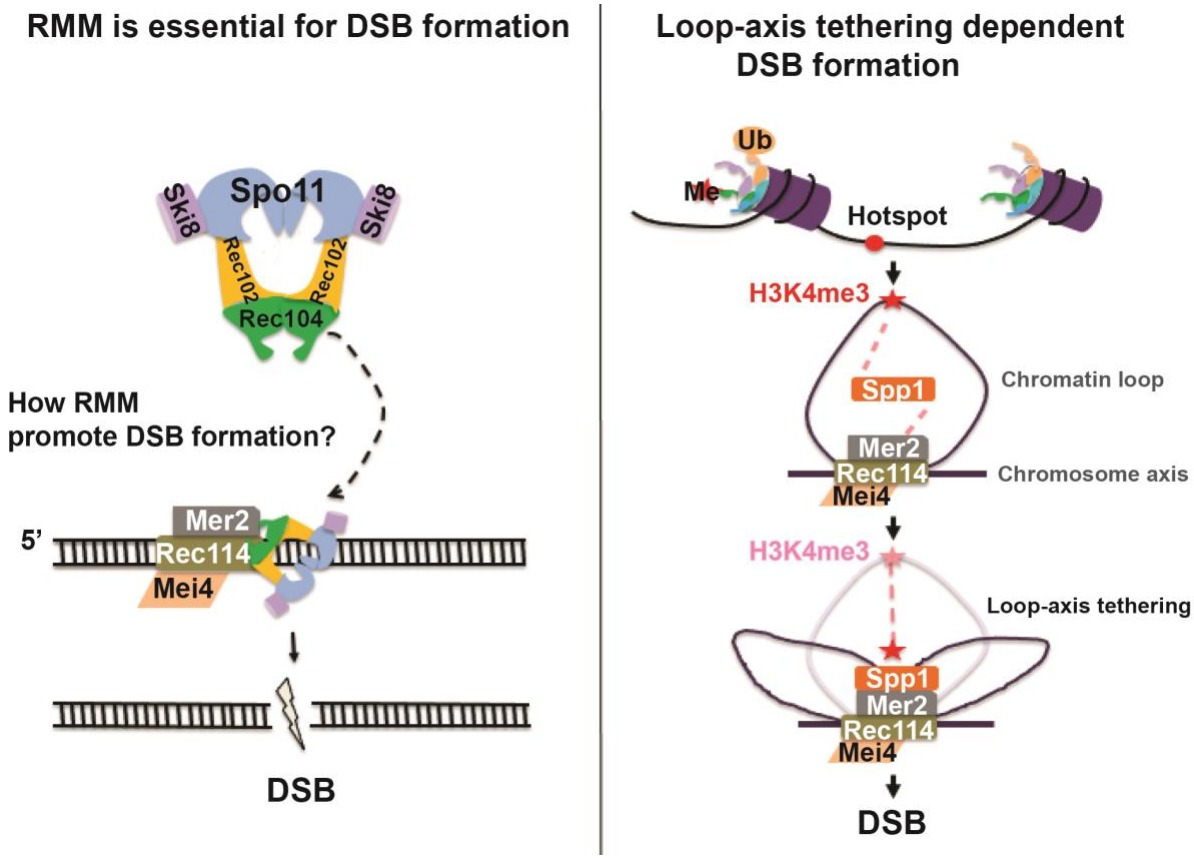

Fig. IV Left: RMM is essential for DSB formation

(left) Spo11 induces DSBs by forming covalent linkages to double-stranded DNA. Spo11 cannot catalyze DSB formation alone, and additional factors, such as Rec102, Rec104, Rec114, Ski8, Mei4, and Mer2 are required. Rec114, Mei4, and Mer2 form the RMM complex, which binds to the chromosome axis.

Fig. IV Right: loop-axis tethering-dependent DSB formation

(right) Recombination during meiosis occurs nonrandomly on chromosomes. Some regions are called recombination hotspots show a high frequency of DSBs. Histone modifications, such as histone H3K4 methylations, mark the sites of recombination hotspots. The chromosome configuration called loop-axis tethering is also critical for DSB formation. H3K4 methylation for DSB formation is located on chromatin loops. On the other hand, the RMM complex is located on the chromosome axis. Spp1 binds to both methylated H3K4 and Mer2 and tethers loop and axis. With this loop-axis tethering through Spp1, Spo11C induces DSB formation close to the RMM complex.

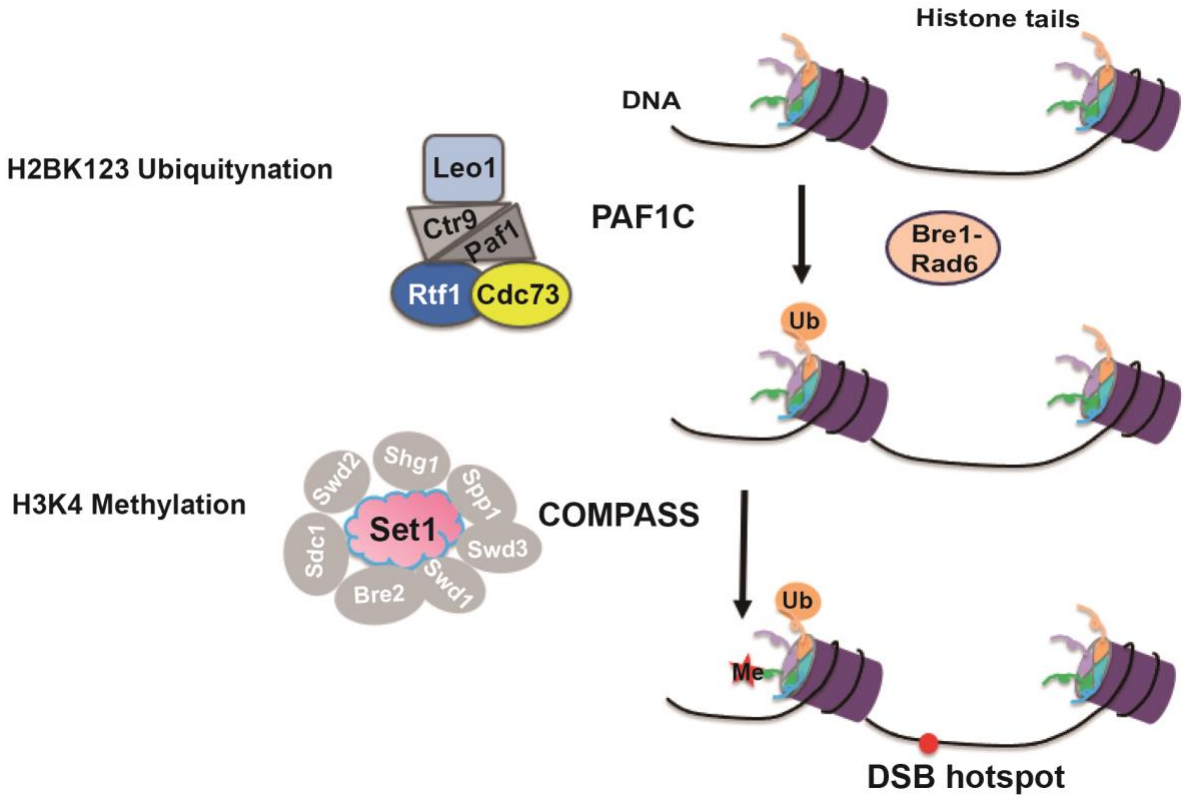

Fig. V Histone modification machinery regulates DSB formation

Set1C/COMPASS methyltransferase mediates histone H3K4 methylation. H2BK123 ubiquitination promotes H3K4 methylation. The E2-E3 pair of Rad6-Bre1 catalyzes ubiquitination which is facilitated by PAF1C.

Chapter II. Materials and Methods

2-1. Strains

All strains used were derived from SK1 background strains MSY831/833 (*MATα/a, ho::LYS2, lys2, ura3, leu2::hisG, trp1::hisG*) and NKY1551 (*MATα/a, ho::LYS2, lys2, ura3, leu2::hisG, his4X-LEU2 (BamHI)-URA3/his4B-LEU2 (MluI), arg-nsp/arg4-bgl*). In this thesis project, all the strains were constructed by the cross and backcross methods. Importantly, to prevent the disorder of genotypes, strains from an MSY background which was in simple genotype were crossed with strains with an NKY background which was in complicated genotype. The plates were incubated at 30 °C for two days, and these plates were replicated to generate corresponding marker plates which were shown in genotype through a commonly used replication method. Selected markers in genotype, replicated from com plate to min plate, replicated to plates of *MATα* and *MAT a* type to confirm the selected mating type. These candidate strains grew well on YPG plates, ensuring that they had normal mitochondria with which to breathe. When marker analysis yielded conflicting results, PCR was performed to confirm the deletion in the marked strain. In this thesis, PCR was used to verify the genotype of *rtf1* and *MER2-myc* in the *rtf1 MER2-myc* strain. The genotypes of each strain are shown in Table 1.

2-2. Tetrad dissection

Haploid strains of the *MATα* and *MATa* type were mixed for 6 hr and incubated for 2 days at 30 °C after streaking onto YPAD mediums. The diploid colonies were transferred onto an SPM plate (0.3% Potassium acetate, 0.02% Raffinose, agar), then incubated for 1-2 days. Under an optical microscope (Zeiss Axioskop 40), the number of the four spore cells is more than 30% of the cells.

Preparation of zymolyase solution for tetrad dissection:
Fifteen microliters of zymolyase solution (100 mg/ml of zymolyase 100T in 850 μl of distilled water, 50 μl of Tris-HCL [pH 7.5], and 100 μl of 20% glucose) was added to 200 μl of ZK buffer (25mM Tris-HCL [7.5], 0.8M KCl), stood at room temperature for 10 min, then added another 300 μl ZK buffer, stored at 4 °C.

Picked appropriate quantity of sample from one colony was added to the solution, mixed thoroughly, and allowed to stand for 30 min at room temperature. It was stored at 4 °C and used within 4 days.

2-3. Yeast transformation (the LiAc Method)

Strains from the -80 °C freezer were revived on YPG for 12 hr and then transferred and streaked out on YPAD plates and incubated at 37 °C for two days. One proper colony was selected from the 2 ml of YPAD liquid medium and incubated overnight. YPAD (50 ml) was added to a 200-ml flask, diluted overnight in YPAD until the OD value was in the range of 0.4-0.6, and incubated at 30 °C while rotated at 230 rpm in a shaker (Innova) for 2.5 to 3 hr. The culture was centrifuged for 3 min at 3000 rpm in a sterilized screw cap tube. The cells were washed twice in sterile distilled water, centrifuged at 3000 rpm for 3 min. Suspended in 1 ml of LiAc/TE (0.1 M LiAc, 1xTE), transferred to a new Eppendorf tube, and centrifuged at 5000 rpm for 1 min. Then, 200 µl of LiAc/TE and 10 µl of carrier DNA (10 mg/ml deoxyribonucleic acid from salmon sperm, Wako Ltd) were added, heated to 95 °C if it was sticky. Fifty microliters of each of the cell cultures were transferred to a new Eppendorf tube, and plasmid or DNA fragments were added to each tube and thoroughly mixed. Then, 350 µl of PEG/LiAc/TE (40% (w/v) PEG4000 and 0.1 M LiAc, 1xTE) was added and mixed thoroughly with inverting the tubes and then incubated with rotation at 30 °C for 1 hr and 42 °C for 15 min in a heat block or water bath. The mixture was cooled in an ice bath for 1 min, then centrifuged at 5000 rpm for 1 min, and then, the supernatant was aspirated. The cells were suspended in 100 µl of PBS or 10:1 TE and spread on selective plates. Specifically, the kanamycin-resistant strain cells were first suspended in 1 ml of YPAD, transferred to 1.5 ml centrifuge tubes, and incubated for 3-6 hr or overnight. The cells were centrifuged at 1500 rpm for 2 min. Then, the cells were suspended in 100 µl of PBS (phosphate-buffered saline) or TE and spread onto a Kanamycin plate.

2-4. Meiotic time course

Diploid yeast strains were revived on YPG plates (1% Bacto yeast extract, 2% Bacto peptone, and 2% glycerol) for 12 hr, streaked out on YPAD plates, and incubated at 30 °C for 2 days to obtain single colonies. One large colony was selected, added to 2

ml of liquid YPAD, and incubated overnight on a rotating machine. Two milliliters of liquid YPAD was added to 200 ml of autoclaved SPS medium (0.5% Bacto yeast extract, 1% Bacto peptone, 0.17% yeast nitrogen base, 1% potassium acetate, 1% potassium hydrogen phthalate, and 0.5% ammonium sulfate), shaken and incubated for 16 hr. The SPS medium samples were collected at 3000 rpm for 2 min, washed with distilled water three times, centrifuged, and pipetted. The cells were suspended in SPM (0.3% potassium acetate and 0.02% raffinose) and incubated at 30 °C while rotating at 230 rpm. Samples were collected at each time point.

2-5. Meiotic nuclear spreads: The lipsol method

Dithiothreitol (DTT, 1 M), zymolyase solution (5 mg/ml, zymolyase 100T, 2% glucose, and 50 mM Tris [pH 7.5]), MES/sorbitol (0.1 M MES [pH 6.5] and 1 M sorbitol), 1% lipsol, and PFA/sucrose (4% PFA [paraformaldehyde], Sigma-Aldrich]), and 3.4% sucrose) were placed on ice. Five milliliters of time course sample was centrifuged at 3000 rpm for 2 min and pipetted the supernatant. One milliliter of ZK buffer and 20 µl of 1 M DTT was added to the sample, gently mixed, incubated for 2 min at room temperature, and pipetted again. Then, 1 ml of ZK buffer and 5 µl of 5 mg/ml zymolyase solution, which was freshly prepared, were added to the sample and incubated at 30 °C for 0.5 hr. The sample mixture was pipetted, washed with 1 ml of MES/Sorbitol, and pipetted again, and then, 400 µl MES/sorbitol was added. Slides were prepared with 20 µl of the sample with 40 µl of PFA/sucrose was added, followed by 80 µl of 1% lipsol; this liquid was spread over the entire surface of the slide, and another 80 µl of PFA/sucrose was added with a glass pipette to cover the slides. The slides were then allowed to dry untouched overnight.

2-6. DAPI staining

Two hundred microliters of DAPI (10 ug/ml) were added to the samples, and the samples were incubated at room temperature in the dark for 0.5 hr, centrifuged at 7000 rpm for 1 min, and pipetted to discard the supernatant. Then 10-30 µl of distilled water was added and mixed. A 4-µl aliquot of a dyed sample was added to a slide, then was covered with a coverslip. The slides with samples were observed under the epifluorescence microscope (BL 51, Olympus), which recorded the images.

2-7. Western blot analysis

During the meiotic time course, 15-ml samples of each strain were collected in tubes, washed with 10 ml of water. Then, 1 ml of 20% TCA (20% (w/v) trichloroacetic acid) was used to wash the samples, and another 200 µl of TCA (20% (w/v) trichloroacetic acid) was added, and the samples were stored at -20 °C. Two-milliliter tubes containing 0.3 ml of 0.5 mM glass beads and 200 ml of stock solution were roughly disrupted by a Yasui Kikai disrupter (Yasui Kikai Co. Ltd., Osaka, Japan) after the samples were fixed. Deal with samples in this shocker for approximately 15 min. Using a heated needle, a hole was pierced at the bottom of new tubes, and the sample tubes were placed onto these new tubes and centrifuged at 3000 rpm for 5 min. The supernatant remaining in the upper tubes was pipetted clearly, and 180 µl of SDS (sodium dodecyl sulfate) sample buffer was added and mixed thoroughly. After that, 100 µl Tris-HCl [pH 8.8] was added until the samples turned blue. The cells were incubated at 95 °C for 2 min and stored frozen in liquid nitrogen.

SDS-PAGE:

An 8% electrophoresis resolution gel (4.6 ml of H_2O, 2.7 ml of 30% acrylamide mix (29:1), 2.5 ml of 1 M Tris-HCl [pH 8.8], 0.1 ml of 10% SDS, 0.1 ml of 10% ammonium sulfate, and 0.006 ml of TEMED) was prepared to separate proteins larger than 35 kDa. A 15% electrophoresis resolution gel (2.3 ml of H_2O, 5.0 ml of 30% acrylamide mix (29:1), 2.5 ml of 1 M Tris-HCL [PH8.8], 0.1 ml of 10% SDS, 0.1 ml of 10% ammonium sulphate, and 0.004 ml of TEMED) was prepared to separate proteins smaller than 20 kDa. A 5% stacking gel (2.1 ml of H_2O, 0.5 ml of 30% acrylamide mix (29:1), 0.38 ml of 1 M Tris-HCl [pH 6.8], 0.03 ml of 10% SDS, 0.03 ml of 10% ammonium sulfate, 0.003 ml of TEMED) was also prepared. The SDS (sodium dodecyl sulfate) electrophoresis machine was operated at 200v, 30-50mA for 1-2 hr until the loading dye line reached the bottom. Then, the identity of the proteins was confirmed by western blotting with anti-H3K4me, anti-H3K4me2, anti-H3K4me3, and anti-H3K79me3 antibodies. The diluted concentration of antibodies is shown in Table 2.

2-8. Immunostaining of meiotic chromosome spreads

Slides with chromosomes spread onto them were prepared and dried well as described in sections 2-5. These slides were dipped in 0.2% Photo-Flo solution (Photo-Flo 200 solution, Kodak) for 2 min in a Coplin jar. The slides were air-dried for 5-10 min and blocked for 15 min with 0.5 ml TBS/BSA (1x TBS [20 mM Tris, pH 7.5, and 0.15 M NaCl], 1% BSA [bovine serum albumin, Sigma]). The blocking buffer was drained onto a paper towel, and 90 µl of primary antibody solution (1:200 dilution of antiserum in TBS/BSA) was added to the slides, which were then covered with a coverslip and incubated overnight at 4 °C for 2 hr at room temperature in a moist chamber. The coverslips were removed by submerging the slides into wash buffer (1x TBS) at a 45 °C angle. The slides were washed 3 times with 1x TBS in a Coplin jar for 10 min each time. Then, 90 µl of secondary antibody solution (1:2000 dilution of fluorochrome-conjugated IgG in TBS/BSA) was added to the slides and incubated for 2 hr at room temperature in a dark moist chamber. The coverslips were removed, and the slides were washed as described above and then washed with water for 2 min. The slides were dried completely, and 15 µl (three drops) of mounting medium (VECTASHIELD with 0.2 mg/ml DAPI) was added to the slides. The slides were covered with coverslips, sealed with nail polish, and stored in a dark box. The samples were observed under an epifluorescence microscope (BX51; Olympus, Tokyo, Japan) with a 100× objective (NA1.3). Images were captured by CCD camera (CoolSNAP; Roper, Sarasota, FL, USA) and afterwards processing using IP lab and/or iVision (Sillicon, Austin, TX,USA) and Photoshop (Adobe, San Jose, CA, USA) software tools. The dilution of the antibodies is shown in Table 3. For analyzing the kinetics of positive cells, at least 100 positive cells were counted at each time point. In this thesis project, 42 cells in each experiment were counted for the positive foci number analysis.

2-9. Yeast genomic DNA preparation

Fifteen milliliters of SPM samples or one-half of a colony in 2 ml liquid YPAD was incubated at 30 °C overnight. Then, the samples were centrifuged and cells were suspended in 500 µl of zymolyase buffer and incubated at 37 °C for 30 min. Then, 5 µl of proteinase K (10 mg/ml) and 100 µl lysing buffer were added and mixed, then incubated at 65 °C for 1 hr. During this time, the sample was mixed at least one time. Next, 100 µl of 5 M potassium acetate was mixed and placed on ice for 15 min and centrifuged at 15000 rpm for 10 min. At the same time, 100% (V/V) cold EtOH was

added to new centrifuge tubes. The supernatant was added to the tubes containing cold EtOH, inverted gently 5 times, and centrifuged at 12000 rpm for 2 min. The supernatant was discarded, and the precipitate was washed with 1 ml of 70% EtOH, washed with 1 ml of 100% EtOH again to obtain additional DNA. The DNA was dried in a vacuum centrifugal concentrator (Martin Christ) for 10 min or air-dried for 1 hr. After that, 200 µl 1xTE was added and dissolved DNA overnight.

Chapter III. Results

3-1 *rtf1* deletion is synthetic defective with *REC114-myc* in DSB formation

Rec114, Mer2, and Mei4 form a complex called the RMM complex, which is located on the chromosome axis and produces DSBs [48]. The RMM interacts with the Spo11 complex to trigger its catalytic activity [50, 69]. As shown previously [70], the spore viability of deletions of *rec114*, *rec102*, or *spo11* was less than 5%. Therefore, to analyze the interaction between genes in histone modification and DSB formation factors, in this thesis, I used the myc-tagged alleles of both *REC114* and *MER2* genes. Previous studies showed that the *REC114-9myc* and *MER2-13myc* (hereafter, *REC114-myc* and *MER2-myc*, respectively as shown below) had synthetic interaction with mutants of *RED1* and *HOP1*, which encoded a component of axial element [49], and determined the distribution of DSBs along chromosomes in yeast [71, 72]. Therefore, it is interesting to analyze the genetic interaction between mutations in the histone modification machinery and tagged-alleles of RMM components.

For this, I combined a deletion mutation of Rtf1 subunit in PAF1C with *REC114-myc*, First, I checked the spore viability of the *rtf1 REC114-myc* strain by dissecting 300 tetrads of each strain. In the spore viability analysis, the wild-type strain showed high spore viability at 97 ± 2.1%. Similar to the wild-type strain, the *REC114-myc* strain showed high spore viability of 95.9 ± 2.6%, indicating that the addition of the myc-tag did not affect the function of Rec114, consistent with the previous study [52]. As reported previously [73], the *rtf1* mutant showed slightly reduced spore viability at 75.3 ± 6.6%. However, the double mutant of the homozygous *rtf1 REC114-myc* strain showed a substantial reduction in spore viability, decreasing to 7.8 ± 3.7% (Fig. 1 A), indicating strong genetic interaction between the *rtf1* deletion and the *REC114-myc* alleles. In other words, the Rtf1 protein plays an important role in viable spore formation in the presence of a myc-tag in the C-terminus of Rec114.

To characterize the meiotic defect seen in the *rtf1 REC114-myc* strain, I analyzed the progression of meiosis by assessing DAPI-stained cells. DAPI is a dye that binds to DNA, and with this dye, I could observe the number of nuclei in a cell. After induction of meiosis by incubating yeast cells with SPM, cells were collected and stained with DAPI. In the wild-type strain, meiosis I began at approximately 5 hr. The *REC114-myc*

strain showed half an hour delay to enter MI than the wild-type strain. The *rtf1* deletion mutant delayed entering MI by 2 hr. While *rtf1 REC114-myc* strain entered MI in a similar timing with the wild-type strain that was 5 hr, but earlier than both *REC114-myc* and *rtf1* mutants (Fig. 1 B). These findings indicated a genetic interaction between *REC114-myc* and *rtf1* alleles; *REC114-myc* rescued the induced MI delay by *rtf1* deletion.

To determine the cause of the genetic interaction between *rtf1* and *REC114-myc,* we analyzed the formation and repair of DSBs indirectly by analyzing the number of Rad51 foci using the immuno-staining analysis of chromosome spreads from meiotic yeast cells by anti-Rad51 antibody. Rad51 is a recombinase that binds to ssDNA at DSB sites. Immuno-staining showed dotty staining of Rad51 called Rad51 foci (Fig. 1 B). Rad51 foci are good markers of DSB formation and repair [74]. In the wild-type, Rad51 appeared at 3 hr, peaked at 4 hr, gradually disappeared after 5 hr (Fig. 1 C). The number of Rad51-positive cells peaked at 4 hr with 77.1 ± 1.4%. In the *REC114-myc* strain which delayed Rad51-focus formation slightly, the number of Rad51-positive nuclei peaked at 6 hr with 41.8 ± 10.9%. In the *rtf1*, the number of Rad51-positive cells peaked at 5 hr with 54.7 ± 3.8%. Importantly, the *rtf1 REC114-myc* strain showed little Rad51 foci on the spreads, indicating a synthetic defect leading to a reduced number of Rad51 foci, suggesting that the number of formed DSBs was largely reduced in the *rtf1 REC114-myc* strain (Fig. 1 C). The reduced spore viability could be explained by this large reduction in the DSB formation during meiotic recombination in the mutant.

I also counted the number of Rad51 foci in a spread in each strain and constructed a dot graph. One hundred and twenty-six cells (42 cells in each experiment) of each strain were randomly counted. The cells with more than 5 foci per nucleus were counted as positive cells. The negative cells were not calculated in the mean number of Rad51 foci analysis. At the 4-hr time point, the number of Rad51 foci in the wild-type had a mean value of 36.2 ± 17.1, and in the *REC114-myc* strain, the number of foci was reduced to 16.7 ± 9.0 (p<0.0001 compared to the wild-type, Mann-Whitney *U* test), this suggested a weak defect of Rec114 function by the addition of tag. *rtf1* deletion reduced the number of Rad51 foci to 23.1 ± 11.7 (p<0.0001 compared to the wild-type, Mann-Whitney *U* test), consistent with the previous report [58]. Although the *rtf1 REC114-myc* strain showed a few focus-positive spread in which an average number of foci was 15.1 ± 6.9 (n=8; Fig. 1 F). Since we did not include Rad51-focus

negative cells, this number is over-interpreted. If the number is recollected, an average number of Rad51 foci in a cell is 26.7, 9.3, 14.1, and 1.0 in wild-type, *REC114-myc*, *rtf1,* and *rtf1 REC114-myc* cells, respectively.

To check the *rtf1* deletion affect the Rec114-myc localization on meiotic chromosomes, I also stained the spreads with the Anti-myc antibody. The staining revealed the localization of the Rec114 protein on meiotic chromosomes as focus staining (Fig. 1C), consistent with the previous study [75]. *REC114-myc* did not colocalize with Rad51 foci, which suggests the DSB sites marked with Rad51 on chromatin loops are spatially separated from chromosome axes with Rec114 on the chromosome spread. In the *REC114-myc* strain, Rec114 foci appeared at 3 hr, and reached to plateau at 4 and gradually disappeared after 8 hr (Fig. 1E). In the *REC114-myc* cells, the myc-positive focus number peaked at 67.9 ± 23.4% at 6 hr. Importantly, in *rtf1 REC114-myc*, the *rtf1* deletion did not affect antibody staining of Rec114. The myc-positive focus number peaked at 4 hr with 58.7 ± 11.8% positive foci (Fig. 1 C, E).

The number of myc foci was also counted. In the myc-focus number analysis, *REC114-myc* showed a mean value of 22.8 ± 15.0 foci (in positive nuclei) at 4 hr. The *rtf1 REC114-myc* combination did not affect the myc-focus number with the mean value of 25.6 ± 22.2. Therefore, the myc-tag added to Rec114 did not affect the localization of the protein to the chromosome axis (Fig. 1 G).

Figure 1

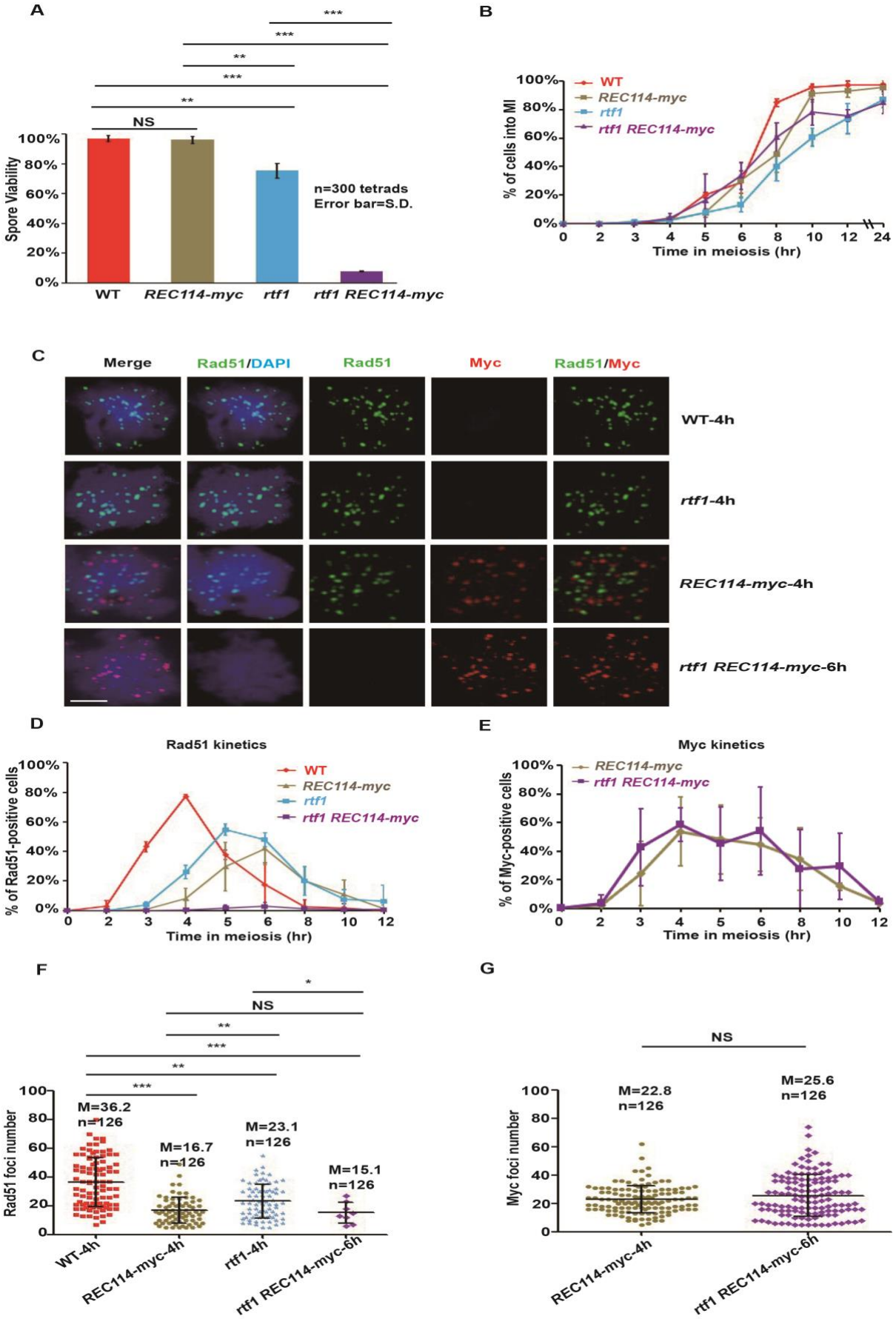
A
***
***
**
***
**
NS
100%
80%
60%
40%
20%
0%
Spore Viability
n=300 tetrads
Error bar=S.D.
WT
REC114-myc
rtf1
rtf1 REC114-myc
B
100%
80%
60%
40%
20%
0%
% of cells into MI
WT
REC114-myc
rtf1
rtf1 REC114-myc
0 2 3 4 5 6 8 10 12 24
Time in meiosis (hr)
C
Merge
Rad51/DAPI
Rad51
Myc
Rad51/Myc
WT-4h
rtf1-4h
REC114-myc-4h
rtf1 REC114-myc-6h
D
Rad51 kinetics
100%
80%
60%
40%
20%
0%
% of Rad51-positive cells
WT
REC114-myc
rtf1
rtf1 REC114-myc
0 2 3 4 5 6 8 10 12
Time in meiosis (hr)
E
Myc kinetics
100%
80%
60%
40%
20%
0%
% of Myc-positive cells
REC114-myc
rtf1 REC114-myc
0 2 3 4 5 6 8 10 12
Time in meiosis (hr)
F
*
NS
**
***
**
***
100
80
60
40
20
0
Rad51 foci number
M=36.2
n=126
M=16.7
n=126
M=23.1
n=126
M=15.1
n=126
WT-4h
REC114-myc-4h
rtf1-4h
rtf1 REC114-myc-6h
G
NS
100
80
60
40
20
0
Myc foci number
M=22.8
n=126
M=25.6
n=126
REC114-myc-4h
rtf1 REC114-myc-6h

Figure 1. *REC114-myc* shows a synthetic defect with *rtf1* in Rad51 focus formation

(A). Spore viability analysis of the wild-type (ZYY1028), *rtf1* (ZYY389), *REC114-myc* (ZYY411), and *rtf1 REC114-myc* (ZYY389) strains. Three hundred tetrads were assessed for each independent analysis, and the error bars indicate the mean values ± standard deviation (S.D.) on basis of three independent experiments. * $p<0.05$; ** $p<0.01$; *** $p<0.001$. NS indicates not significant. The data were analyzed by the Wilcoxon Mann-Whitney *U* test.

(B). DAPI staining analysis of each strain. One hundred cells were counted randomly at each time point. Each plotted value represents the mean value ± standard deviation (S.D.) based on three independent time courses. A parallel slash indicates the period from 12 hr to 24 hr.

(C). Cytology immunostaining of Rad51 (green), myc (red), and DAPI (blue). The bar indicates two micrometers.

(D). Kinetics of Rad51 positive cells. One hundred cells were counted randomly in three independent experiments. Each plotted value represents the mean value ± standard deviation (S.D.).

(E). Kinetics of myc-positive cells. A total of 100 cells were randomly counted in three independent experiments. Each plotted value represents the mean value ± standard deviation (S.D.) on basis of three independent time courses.

(F). Number of Rad51 foci. Forty-two cells were randomly counted in each of three independent experiments (n=126; 42x3). The black line indicates the mean value ± standard deviation (S.D.) for 126 cells. * $p<0.05$; ** $p<0.01$; *** $p<0.001$. NS indicates not significant. The data were analyzed by the Wilcoxon-Mann-Whitney *U* test.

(G). A number of myc foci. Forty-two cells were randomly counted in each of three independent experiments (n=126; 42x3). The black line indicates the mean value ± standard deviation (S.D.) for 126 cells. * $p<0.05$; ** $p<0.01$; *** $p<0.001$. NS indicates not significant. The data were analyzed using the Wilcoxon-Mann-Whitney *U* test.

3-2. The *rtf1* deletion strain shows a synthetic defect with *MER2-myc* in DSB formation

I extended the observation of the synthetic defects in the *rtf1* deletion and myc-tagged *REC114* alleles and examined the relationships between *rtf1* and another component of the RMM complex, Mer2 protein, and generated a myc-tagged version of Mer2. I also found a strong genetic interaction in the double mutant of *rtf1 MER2-myc*. The spore viability of the *MER2-myc* strain was 80.0%. On the other hand, the *rtf1 MER2-myc* showed a large reduction of 0.5 ± 0.1%, indicating a strong synthetic defect between *rtf1* deletion and *MER2-myc* allele in spore viability (Fig. 2 A).

DAPI staining analysis showed that *MER2-myc* enters and finishes MI at times similar to those of the wild-type. While, *rtf1 MER2-myc* enters 1 hr earlier than wild-type control, and 2 hr earlier than *rtf1* mutant (Fig. 2 B), indicating the myc-tagging of Mer2 rescued the *rtf1*-induced defect in MI progression.

In the Rad51 staining analysis, the number of Rad51-positive nuclei in the *MER2-myc* strain peaked at 5 hr with similar levels as the wild-type. The *rtf1 MER2-Myc* strain showed a large decrease in Rad51-positive cells (Fig. 2 C, D), suggesting defective DSB formation in the mutant, which may explain the defective spore viability. To see the Rad51 foci number of each cell, I analyzed it in a similar way, as shown in Fig. 1. At the 4-hr time point, in the wild-type, the mean number of Rad51-positive foci was 28.9 ± 18.1, the mean number of Rad51-positive foci in the *MER2-myc* strain was 18.2 ± 9.5, and in the *rtf1* strain, it was 23.8 ± 9.6. However, in the *rtf1 MER2-myc* strain, the number of Rad51 positive foci was only 8.7 ± 3.9. An average number of Rad51 foci in a cell is 28.9, 10.1, 21.1, and 0.5 in wild-type, *MER2-myc, rtf1,* and *rtf1 MER2-myc* cells, respectively.

The *rtf1* did not affect the localization of *MER2-myc* on meiotic chromosomes compared to that of the control (Fig. 2 C, E). Like Rec114 foci, Mer2-myc showed focus staining, which did not colocalize with Rad51 foci. At the 4-hr time point, the myc-positive number in *MER2-myc* and *rtf1 MER2-myc* strains were similar; the mean value in the *MER2-myc* and the *rtf1 MER2-myc* strains was 28.5 ± 9.5 and 29.3 ± 16.2, respectively. Taken together, these results indicate that the *rtf1* deletion allele genetically interacts with *MER2-myc* in meiotic DSB formation as with the *REC114-myc*. The effect of the *rtf1* is not through the localization of two RMM components,

Rec114 and Mer2 since either deletion does not alter the localization of the myc-tagged proteins.

Figure 2

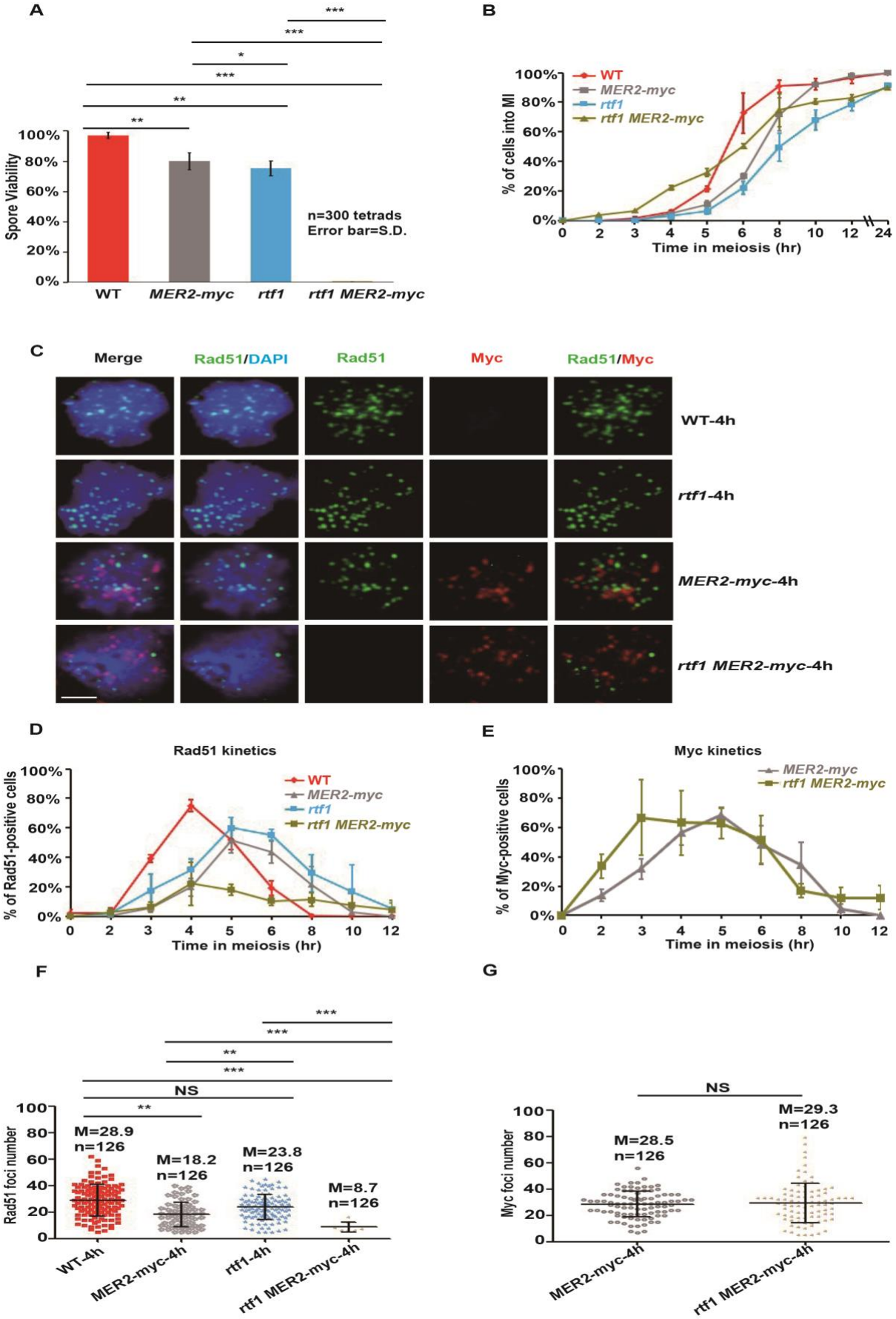
A
***
***
*
***
**
**
100%
80%
60%
40%
20%
0%
Spore Viability
n=300 tetrads
Error bar=S.D.
WT
MER2-myc
rtf1
rtf1 MER2-myc
B
100%
80%
60%
40%
20%
0%
% of cells into MI
WT
MER2-myc
rtf1
rtf1 MER2-myc
0 2 3 4 5 6 8 10 12 24
Time in meiosis (hr)
C
Merge
Rad51/DAPI
Rad51
Myc
Rad51/Myc
WT-4h
rtf1-4h
MER2-myc-4h
rtf1 MER2-myc-4h
D
Rad51 kinetics
100%
80%
60%
40%
20%
0%
% of Rad51-positive cells
WT
MER2-myc
rtf1
rtf1 MER2-myc
0 2 3 4 5 6 8 10 12
Time in meiosis (hr)
E
Myc kinetics
100%
80%
60%
40%
20%
0%
% of Myc-positive cells
MER2-myc
rtf1 MER2-myc
0 2 3 4 5 6 8 10 12
Time in meiosis (hr)
F
***
***
**
***
NS
**
100
80
60
40
20
0
Rad51 foci number
M=28.9
n=126
M=18.2
n=126
M=23.8
n=126
M=8.7
n=126
WT-4h
MER2-myc-4h
rtf1-4h
rtf1 MER2-myc-4h
G
NS
100
80
60
40
20
0
Myc foci number
M=28.5
n=126
M=29.3
n=126
MER2-myc-4h
rtf1 MER2-myc-4h

Figure 2. *MER2-myc* shows a synthetic defect with *rtf1* in Rad51 focus formation
(A). Spore viability analysis of the wild-type (ZYY1028), *rtf1* (ZYY389), *MER2-myc* (ZYY893), and *rtf1 MER2-myc* (ZYY874) strains. I analyzed 300 tetrads for each independent experiment, and the error bars indicate the standard deviation (S.D.) on basis of three independent time courses. * $p<0.05$; ** $p<0.01$; *** $p<0.001$. NS indicates not significant. The data were analyzed by the Wilcoxon Mann-Whitney *U* test.
(B). DAPI staining analysis of each strain. One hundred cells were counted randomly at each time point. Each plotted value represents the mean value ± standard deviation (S.D.) on basis of three independent time courses. A parallel slash indicates a period from 12 hr to 24 hr.
(C). Cytology immunostaining of Rad51 (green), myc (red), and DAPI (blue). The bar indicates two micrometers.
(D). Kinetics of Rad51-positive cells. One hundred cells were counted randomly in three independent experiments. Each plotted value represents the mean value ± standard deviation (S.D.).
(E). Kinetics of myc-positive cells. A total of 100 cells were randomly counted in three independent experiments. Each plotted value represents the mean value ± standard deviation (S.D.) of three independent time courses.
(F). Number of Rad51 foci. Forty-two cells were randomly counted in each of three independent experiments (n=126; 42x3). The black line indicates the mean value ± standard deviation (S.D.) of 126 cells. * $p<0.05$; ** $p<0.01$; *** $p<0.001$. NS indicates not significant. The data were analyzed by the Wilcoxon-Mann-Whitney *U* test.
(G). A number of myc foci. Forty-two cells were randomly counted in each of three independent experiments (n=126; 42x3). The black line indicates the mean value ± standard deviation (S.D.) of 126 cells. * $p<0.05$; ** $p<0.01$; *** $p<0.001$. NS indicates not significant. The data were analyzed by the Wilcoxon-Mann-Whitney *U* test.

3-3. *cdc73* shows a synthetic defect with *REC114-myc* in DSB formation

The PAF1 complex constitutes five subunits: Rtf1, Cdc73, Ctr9, Leo1 and Paf1 [57]. *RTF1* and *CDC73* are very important in H2BK123 ubiquitination and H3K4 methylation. The *cdc73* single mutant showed a wild-type level of spore viability of 98.8%. When examining the spore viability of the homozygous *cdc73 REC114-myc* combination, I obtained dead spores (Fig. 3 A). These indicate a strong synthetic interaction between *cdc73* and *REC114-myc* in spore viability.

In the DAPI staining analysis, the single mutant *cdc73* entered MI at 4.5 hr, earlier than the wild-type. *cdc73 REC114-myc* showed delayed entrance into MI by 6.5 hr (Fig. 3 B). The kinetic analysis of Rad51-focus positive cells in the wild-type peaked at 4 hr with 72.6 ± 1.3%. In the *REC114-myc cells*, peaks were observed at 5 hr with 42.1 ± 18.7%. In *cdc73*, peaks were observed at 4 hr with 63.0 ± 8.1%. In *cdc73 REC114-myc*, the peaks observed at 5 hr were largely decreased, and 6.6 ± 4.6% were Rad51 focus-positive cells, suggesting that there was a synthetic defect in DSB formation in *cdc73 REC114-myc* (Fig. 3 C, D). Moreover, the number of Rad51 foci in one cell of the *cdc73 REC114-myc* strain decreased to 6.8 ± 1.5 (Fig. 3 F). The myc number in each cell had a mean value of 21.8 ± 15.6 in the *REC114-myc* strain and 27.3 ± 19.3 in the *cdc73 REC114-myc* strain (Fig. 3 G). An average number of Rad51 foci in a cell is 24.6, 10.0, 10.7, and 0.21 in wild-type, *REC114-myc, cdc73,* and *cdc73 REC114-myc* cells, respectively.

In Rec114 localization analysis, the *cdc73 REC114-myc* strain showed a peak of myc-positive cells at 5 hr with 51.7 ± 18.6%, which is similar to that in the *REC114-myc* control strain with 46.9 ± 18.3% (Fig. 3 C, E). These results indicate that the deletion of the PAF1C component *CDC73* shows a strong synthetic defect with *REC114-myc* while the *cdc73* deletion does not affect the localization of *REC114-myc* to chromosome axes.

Figure 3

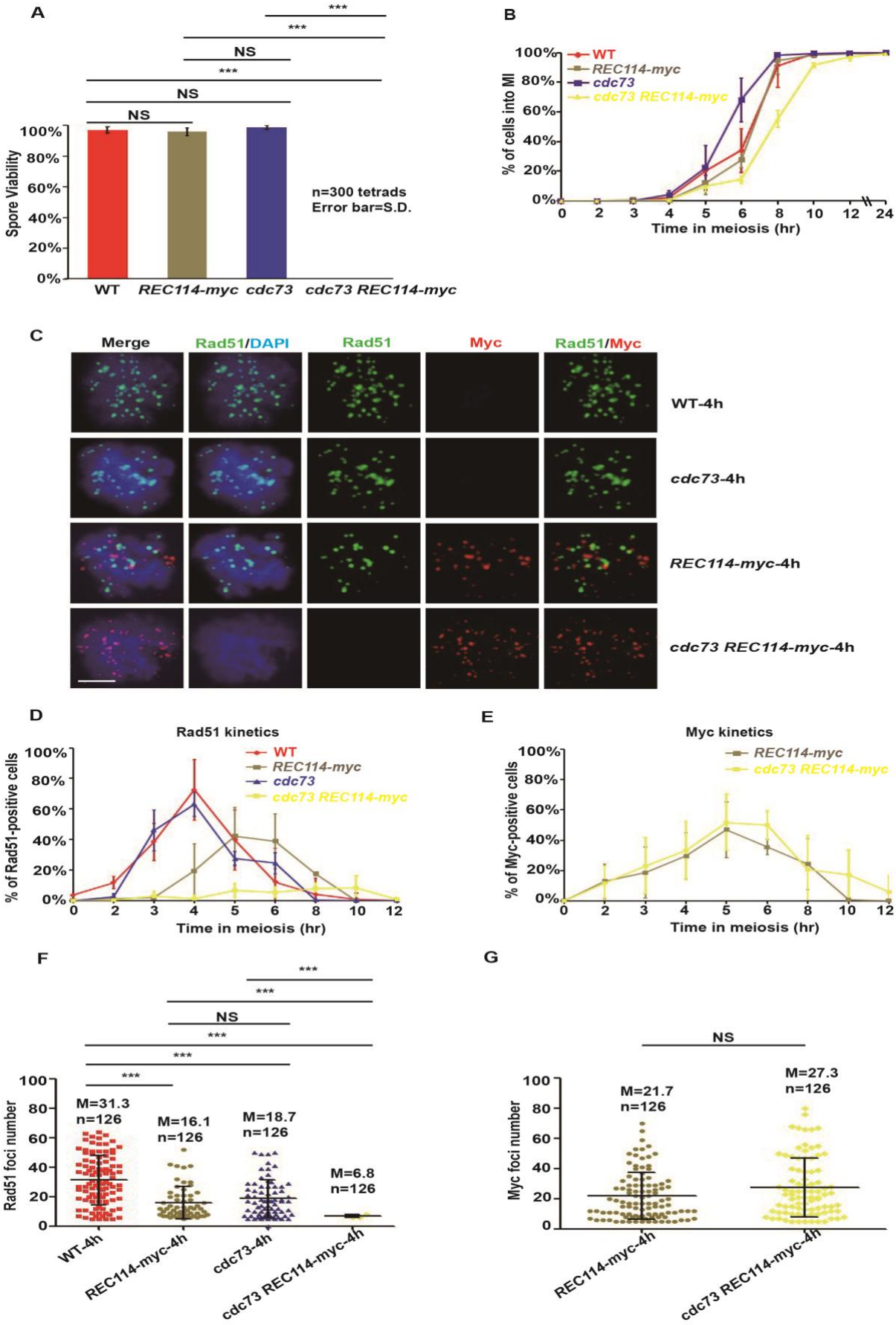
A
***
***
NS
***
NS
NS
Spore Viability
100%
80%
60%
40%
20%
0%
n=300 tetrads
Error bar=S.D.
WT
REC114-myc
cdc73
cdc73 REC114-myc
B
WT
REC114-myc
cdc73
cdc73 REC114-myc
% of cells into MI
Time in meiosis (hr)
C
Merge
Rad51/DAPI
Rad51
Myc
Rad51/Myc
WT-4h
cdc73-4h
REC114-myc-4h
cdc73 REC114-myc-4h
D
Rad51 kinetics
% of Rad51-positive cells
Time in meiosis (hr)
E
Myc kinetics
% of Myc-positive cells
Time in meiosis (hr)
F
Rad51 foci number
M=31.3
n=126
M=16.1
n=126
M=18.7
n=126
M=6.8
n=126
WT-4h
REC114-myc-4h
cdc73-4h
cdc73 REC114-myc-4h
G
NS
Myc foci number
M=21.7
n=126
M=27.3
n=126
REC114-myc-4h
cdc73 REC114-myc-4h

Figure 3. *cdc73* has a strong synthetic defect with *REC114-myc* during Rad51 focus formation

(A). Spore viability analysis of the wild-type (ZYY1028), *cdc73* (ZYY811), *REC114-myc* (ZYY411), and *cdc73 REC114-myc* (ZYY736) strains. A total of 300 tetrads were counted for each independent analysis, and the error bars indicate the standard deviation (S.D.) based on three independent experiments. * $p<0.05$; ** $p<0.01$; *** $p<0.001$. NS indicates not significant. The data were analyzed by the Wilcoxon Mann-Whitney *U* test.

(B). DAPI staining analysis of each strain. One hundred cells were randomly counted at each time point. Each error bar indicates standard deviation (S.D.) on basis of three independent time courses. A parallel slash indicates a period from 12 hr to 24 hr.

(C). Cytology immunostaining of Rad51 (green), myc (red), and DAPI (blue). The bar indicates two micrometers.

(D). Kinetics of Rad51-positive cells. One hundred cells were counted randomly in three independent experiments. Each plotted value represents the mean value ± standard deviation (S.D.).

(E). Kinetics of myc-positive cells. A total of 100 cells were randomly counted in three independent experiments. Each plotted value represents the mean value ± standard deviation (S.D.) based on three independent time courses.

(F). Number of Rad51 foci. Forty-two cells were randomly counted in each of three independent experiments (n=126; 42x3). The black line indicates the mean value ± standard deviation (S.D.) of 126 cells. * $p<0.05$; ** $p<0.01$; *** $p<0.001$. NS indicates not significant. The data were analyzed the sing Wilcoxon-Mann-Whitney *U* test.

(G). A number of myc foci. Forty-two cells were randomly counted in each of three independent experiments (n=126; 42x3). The black line indicates the mean value ± standard deviation (S.D.) of 126 cells. * $p<0.05$; ** $p<0.01$; *** $p<0.001$. NS indicates not significant. The data were analyzed using the Wilcoxon-Mann-Whitney *U* test.

3-4. The *set1* deletion shows a synthetic defect with *REC114-myc* in DSB formation

Since the PAF1 complex affected histone modification such as H3K4 methylation through ubiquitination of H2BK123, next I checked the genetic interaction between *REC114-myc* and the deletion of *SET1* gene, which encodes the catalytic component of H3K4 methyltransferase complex, COMPASS.

As reported previously [58], the spore viability of the *set1* strain (94.9 ± 2.6%) was similar to that of the wild-type strain (97 ± 2.1%) and *REC114-myc* (95.9 ± 2.6%) control. Importantly, the *set1 REC114-myc* strain showed slightly decreased spore viability at 76.1 ± 9.6%, indicating a weak interaction between *set1* and *REC114-myc* in spore viability (Fig. 4 A).

In the DAPI-staining analysis, the *set1* strain entered MI at 6.0 hr, which was delayed compared with the controls of wild-type and *REC114-myc*. The *set1 REC114-myc* strain showed a slight delay in entering MI at 5.5 hr compared to the controls, but earlier than the *set1* mutant (Fig. 4 B).

The kinetics of Rad51 focus-positive cells in the *set1* strain showed a peak at 6 hr with 51.5 ± 12.8%. In the *set1 REC114-myc* strain, the number of Rad51-positive cells peaked at 10 hr with 10.7 ± 6.7%, a considerable reduction (Fig. 4 C, D). The number of Rad51-positive foci in the *set1* strain showed peaked at 5 hr, and the mean number of Rad51-positive foci was 17.5 ± 8.5, and in the *set1 REC114-myc* strain, the mean number of Rad51-positive foci was decreased to 9.3 ± 5.8 at 5 hr (Fig. 4 F). An average number of Rad51 foci in a cell is 26.9, 7.8, 11.3, and 0.2 in wild-type, *REC114-myc, set1,* and *set1 REC114-myc* cells, respectively. These indicate a synthetic defect in the *set1 REC114-myc* in Rad51 focus formation.

In the Rec114 localization study, the *REC114-myc* strain exhibited a peak of myc-positive cells at 5 hr with 41.3 ± 21.5% while the *set1 REC114-myc* strain showed a peak at 6 hr with 52.2 ± 27.3% (Fig. 4 C, E). The mean value of myc-positive cells in the *REC114-myc* strain and *set1 REC114-myc* strain was 29.2 ± 21.6, and 21.2 ± 15.8, respectively (Fig. 4 G), indicating that the *set1* does not affect Rec114. These results indicate that *set1* has synthetic defects with *REC114-myc* in DSB formation without affecting the localization of *REC114-myc* to chromosome axis in the nucleus.

Figure 4

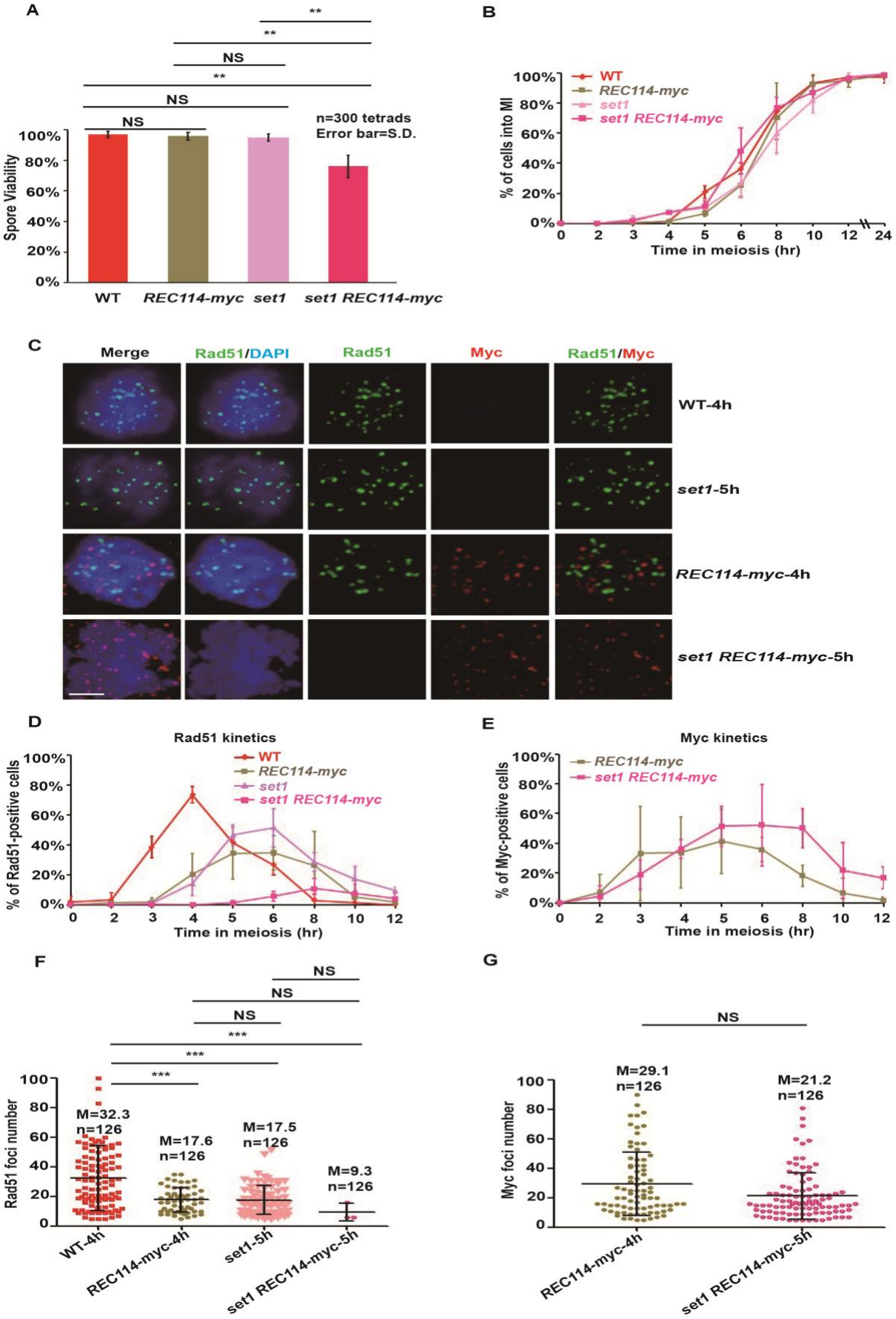
A
**
**
NS
**
NS
NS
n=300 tetrads
Error bar=S.D.
Spore Viability
100%
80%
60%
40%
20%
0%
WT
REC114-myc
set1
set1 REC114-myc
B
WT
REC114-myc
set1
set1 REC114-myc
% of cells into MI
Time in meiosis (hr)
C
Merge
Rad51/DAPI
Rad51
Myc
Rad51/Myc
WT-4h
set1-5h
REC114-myc-4h
set1 REC114-myc-5h
D
Rad51 kinetics
% of Rad51-positive cells
Time in meiosis (hr)
E
Myc kinetics
% of Myc-positive cells
Time in meiosis (hr)
F
NS
NS
NS
***
***
***
Rad51 foci number
M=32.3
n=126
M=17.6
n=126
M=17.5
n=126
M=9.3
n=126
WT-4h
REC114-myc-4h
set1-5h
set1 REC114-myc-5h
G
NS
Myc foci number
M=29.1
n=126
M=21.2
n=126
REC114-myc-4h
set1 REC114-myc-5h

Figure 4. *set1* strongly interacts with *REC114-myc* in Rad51 focus formation

(A). Spore viability analysis of the wild-type (ZYY1028), *set1* (ZYY733), *REC114-myc* (ZYY411), and *set1 REC114-myc* (ZYY812) strains. A total of 300 tetrads were counted for each independent analysis, and each error bar indicates the standard deviation (S.D.) on basis of three independent experiments. * $p<0.05$; ** $p<0.01$; *** $p<0.001$. NS indicates not significant. The data were analyzed by the Wilcoxon Mann-Whitney *U* test.
(B). DAPI staining analysis of each strain. One hundred cells were randomly counted at each time point. Each error bar indicates standard deviation (S.D.) on basis of three independent time courses. A parallel slash indicates a period from 12 hr to 24 hr.
(C). Cytology immunostaining of Rad51 (green), myc (red), and DAPI (blue). The bar indicates two micrometers.
(D). Kinetics of Rad51-positive cells. One hundred cells were counted randomly in three independent experiments. Each plotted value represents the mean value ± standard deviation (S.D.).
(E). Kinetics of myc-positive cells. A total of 100 cells were randomly counted in three independent experiments. Each plotted value represents the mean value ± standard deviation (S.D.) based on three independent time courses.
(F). Number of Rad51 foci. Forty-two cells were randomly counted in each of three independent experiments (n=126; 42x3). The black line indicates the mean value ± standard deviation (S.D.) of 126 cells. * $p<0.05$; ** $p<0.01$; *** $p<0.001$. NS indicates not significant. The data were analyzed by the Wilcoxon-Mann-Whitney *U* test.
(G). A number of myc foci. Forty-two cells were randomly counted in each of three independent experiments (n=126; 42x3). The black line indicates the mean value ± standard deviation (S.D.) of 126 cells. * $p<0.05$; ** $p<0.01$; *** $p<0.001$. NS indicates not significant. The data were analyzed by the Wilcoxon-Mann-Whitney *U* test.

3-5. The *spp1* deletion does not show a genetic interaction with *REC114-myc* in DSB formation

Previous studies have shown that PAF1C- and Set1-dependent histone modification, H3K4 methylation, promotes the interaction of DSB hotspots in chromatin loops with chromosome axes where the RMM complex resides. The above results from my experiments suggest that a defect in loop tethering to the axis due to defective H3K4 methylation mediates genetic interaction with a tagged version of the Rec114 or Mer2 protein. A simple interpretation indicates that loop tethering modulates the activity of the RMM complex on the chromosome axis. Without tethering, the activity of tagged-version of RMM might be compromised. If tethering modulates the RMM functions, once loop tethering was disrupted by a mutation in the *SPP1* gene, which encodes a protein that reads H3K4 methylation and binds to the Mer2 protein, and is essential for tethering [66], I would see there was a similar genetic interaction of a *spp1* deletion mutant and a tagged-allele of RMM. If not, there would be a loop-tethering independent pathway to produce DSBs.

To confirm the interaction between Spp1 and the *REC114-myc* allele, the *spp1* strain was crossed with the *REC114-myc* strain. As reported [73], the spore viability in the *spp1* strain was 95.3 ± 2.8%, which was similar to that in the wild-type. Importantly, the *spp1 REC114-myc* strain shows spore viability of 73.6 ± 9.3%, which is lower than that in the *REC114-myc*, indicating a weak interaction between *spp1* and *REC114-myc* in spore viability (Fig. 5 A). As shown by DAPI staining, the *spp1* strain enters MI at 5.5 hr, and the *spp1 REC114-myc* strain delayed the enter to MI at 6.5 hr compared to the *spp1* (Fig. 5 B).

The *spp1 REC114-myc* strain was analyzed by the immunostaining of chromosome spreads. The *spp1* strain showed peak Rad51-positive foci cells at 6 hr with 38.6 ± 12.6%, and the *spp1 REC114-myc* strain showed a peak of Rad51-positive foci cells at 8 hr with 33.0 ± 8.6% (Fig. 5 C, D). The Rad51-positive foci number in the *spp1* strain was 21.4 ± 10.9, which peaked at 6 hr, while in the *spp1 REC114-myc* mutant, it was 18.6 ± 7.3, which indicated double and single mutants are not significantly different (Fig. 5 F). An average number of Rad51 foci in a cell is 18.2, 8.1, 9.2, and 5.8 in wild-type, *REC114-myc, spp1,* and *spp1 REC114-myc* cells, respectively.

In the myc-positive foci analysis, the peak number of myc-positive foci in the *REC114-myc* strain was 60.6 ± 0.7% at 5 hr, and the *spp1 REC114-myc* strain showed a similar result with 62.1 ± 23.6% at 8 hr (Fig. 5 C, E). The myc-positive focus number in the *REC114-myc* strain was 23.9 ± 18.2 at the 4-hr time point, while in the *spp1 REC114-myc* strain, it was 20.5 ± 13.2 at 6 hr (Fig. 5 G). The *spp1* does not affect Rec114 localization.

These data indicate that different from the *rtf1*, *cdc73*, and *set1*, the *spp1* does not show strong genetic interaction with myc-tagged Rec114 in DSB formation during meiosis. In other words, the Rec114-myc does not interfere with DSB formation in the absence of Spp1. Therefore, the histone modification machinery that involves Rtf1, Cdc73, and Set1 has a loop-tethering independent role in DSB formation.

Figure 5

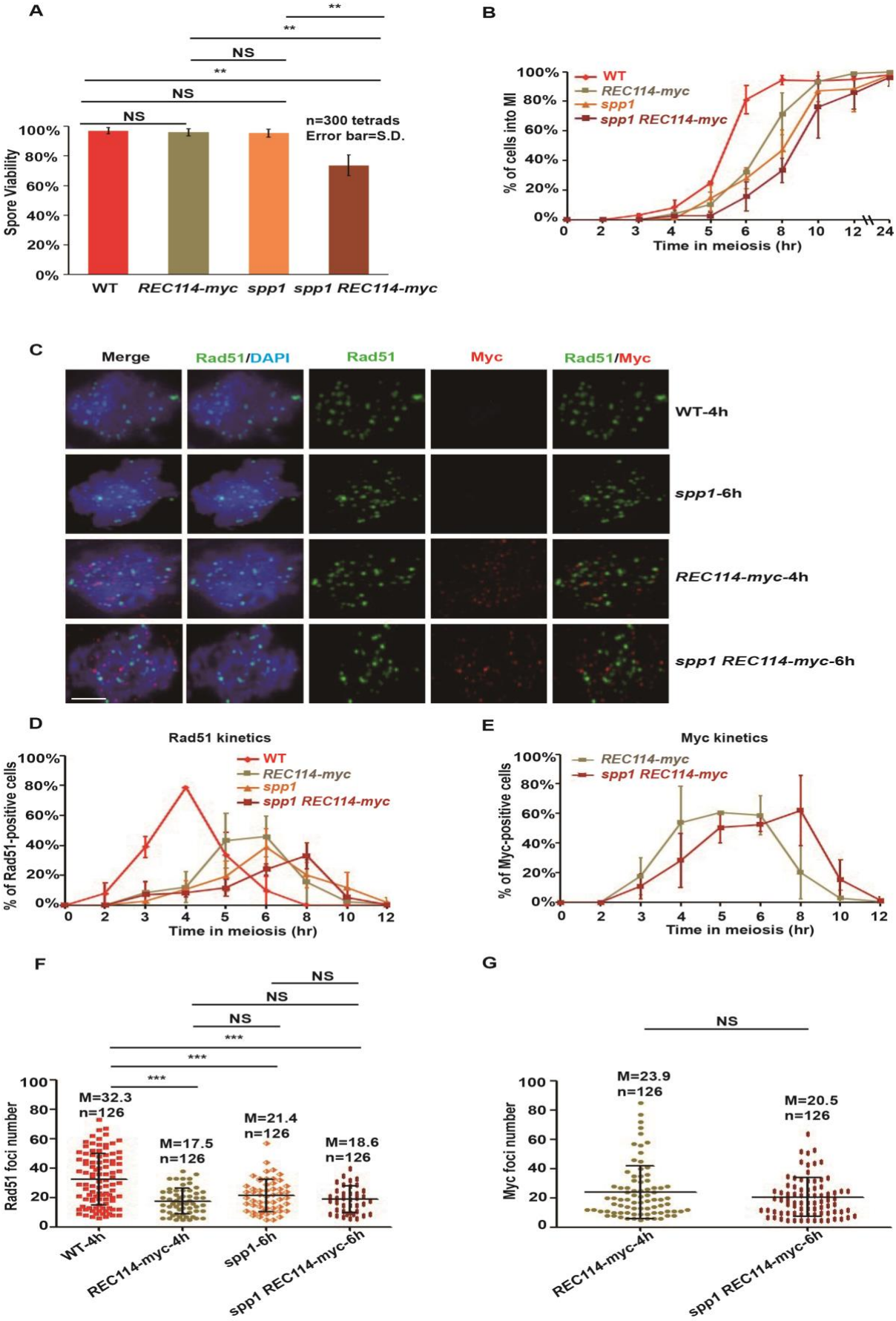
A
**
**
NS
**
NS
NS
n=300 tetrads
Error bar=S.D.
Spore Viability
100%
80%
60%
40%
20%
0%
WT
REC114-myc
spp1
spp1 REC114-myc
B
WT
REC114-myc
spp1
spp1 REC114-myc
% of cells into MI
Time in meiosis (hr)
C
Merge
Rad51/DAPI
Rad51
Myc
Rad51/Myc
WT-4h
spp1-6h
REC114-myc-4h
spp1 REC114-myc-6h
D
Rad51 kinetics
% of Rad51-positive cells
Time in meiosis (hr)
E
Myc kinetics
% of Myc-positive cells
Time in meiosis (hr)
F
NS
NS
NS
***
***
***
Rad51 foci number
M=32.3
n=126
M=17.5
n=126
M=21.4
n=126
M=18.6
n=126
WT-4h
REC114-myc-4h
spp1-6h
spp1 REC114-myc-6h
G
NS
Myc foci number
M=23.9
n=126
M=20.5
n=126
REC114-myc-4h
spp1 REC114-myc-6h

Figure 5. The *spp1* deletion does not show synthetic interaction with *REC114-myc* in Rad51 focus formation

(A). Spore viability analysis of the wild-type (ZYY1028), *spp1* (ZYY892), *REC114-myc* (ZYY411), and *spp1 REC114-myc* (ZYY739) strains. Three hundred tetrads were counted for each independent analysis. Each error bar indicates standard deviation (S.D.) based on three independent experiments. * $p<0.05$; ** $p<0.01$; *** $p<0.001$. NS indicates not significant. The data were analyzed by the Wilcoxon Mann-Whitney *U* test.
(B). DAPI staining analysis of each strain. One hundred cells were randomly counted at each time point. Each plotted value represents the mean value ± standard deviation (S.D.) based on three independent time courses. A parallel slash indicates a period from 12 hr to 24 hr.
(C). Cytology immunostaining of Rad51 (green), myc (red), and DAPI (blue). The bar indicates two micrometers.
(D). Kinetics of Rad51-positive cells. One hundred cells were randomly counted in three independent experiments. Each plotted value represents the mean value ± standard deviation (S.D.).
(E). Kinetics of myc-positive cells. A total of 100 cells were randomly counted in three independent experiments. Each plotted value represents the mean value ± standard deviation (S.D.) based on three independent time courses.
(F). Number of Rad51 foci. Forty-two cells were randomly counted in each of three independent experiments (n=126; 42x3). The black line indicates the mean value ± standard deviation (S.D.) of 126 cells. * $p<0.05$; ** $p<0.01$; *** $p<0.001$. NS indicates not significant. The data were analyzed using the Wilcoxon-Mann-Whitney *U* test.
(G). A number of myc foci. Forty-two cells were randomly counted in each of three independent experiments (n=126; 42x3). The black line indicates the mean value ± standard deviation (S.D.) of 126 cells. * $p<0.05$; ** $p<0.01$; *** $p<0.001$. NS indicates not significant. The data were analyzed by the Wilcoxon-Mann-Whitney *U* test.

3-6. The *spp1* deletion does not show a genetic interaction with *MER2-myc* in DSB formation

Considering the weak interaction between *spp1* and *REC114-myc* and that, I was interested in determining whether *spp1* genetically interacts with Mer2 with the myc-tag. The spore viability of the homozygous strain of *spp1 MER2-myc* was low at 19.7 ± 13.0% (Fig. 6 A), which indicated that there is a strong genetic interaction between *spp1* and *MER2-myc* in DSB formation. As shown in the DAPI analysis, *spp1 MER2-myc* entered MI at 4 hr, which are earlier than the control strains such as wild-type, *spp1,* and *MER2-myc* strains (Fig. 6 B).

In the analysis of the kinetics of Rad51 focus-positive cells, in the *spp1 MER2-myc* strain, the peak was reached at 4.5 hr with 45.0 ± 5.1% Rad51-positive cells (Fig. 6 C, D). In the analysis of the Rad51-positive foci number in the *spp1 MER2-myc* strain, the mean value was 14.2 ± 6.7, with a very slight reduction at the 4 hr time point compared to those of *spp1* and *MER2-myc* strains (Fig. 6 F). An average number of Rad51 foci in a cell is 23.4, 11.0, 13.5, and 7.1 in wild-type, *MER2-4-myc, spp1,* and *spp1 MER2-myc* cells, respectively.

In the kinetics of myc-positive cell analysis, the number in *MER2-myc* strain peaked with 78.5 ± 14.1% myc-positive cells, while *spp1 MER2-myc* strain did with 76.2 ± 4.5% (Fig. 6 C, E). In myc-positive cells, the *MER2-myc* strain showed the mean number with 25.8 ± 17.3 at 4 hr. The myc focus number in the *spp1 MER2-myc* strain was 28.5 ± 21.9 (Fig. 6 G). The *spp1* does not affect the localization of Mer2-myc.

Together, these results indicate that there is little genetic interaction between *spp1* and *MER2-myc* in DSB formation (Rad51 focus formation), a finding similar to that of *spp1* with *REC114-myc*. The mild reduction of the Rad51 focus number could not explain the synthetic defect of the spore viability of the *spp1 MER2-myc* cells. There might be an additional defect that I could not find in meiotic DSB formation of the *spp1 MER2-myc* strain.

Figure 6

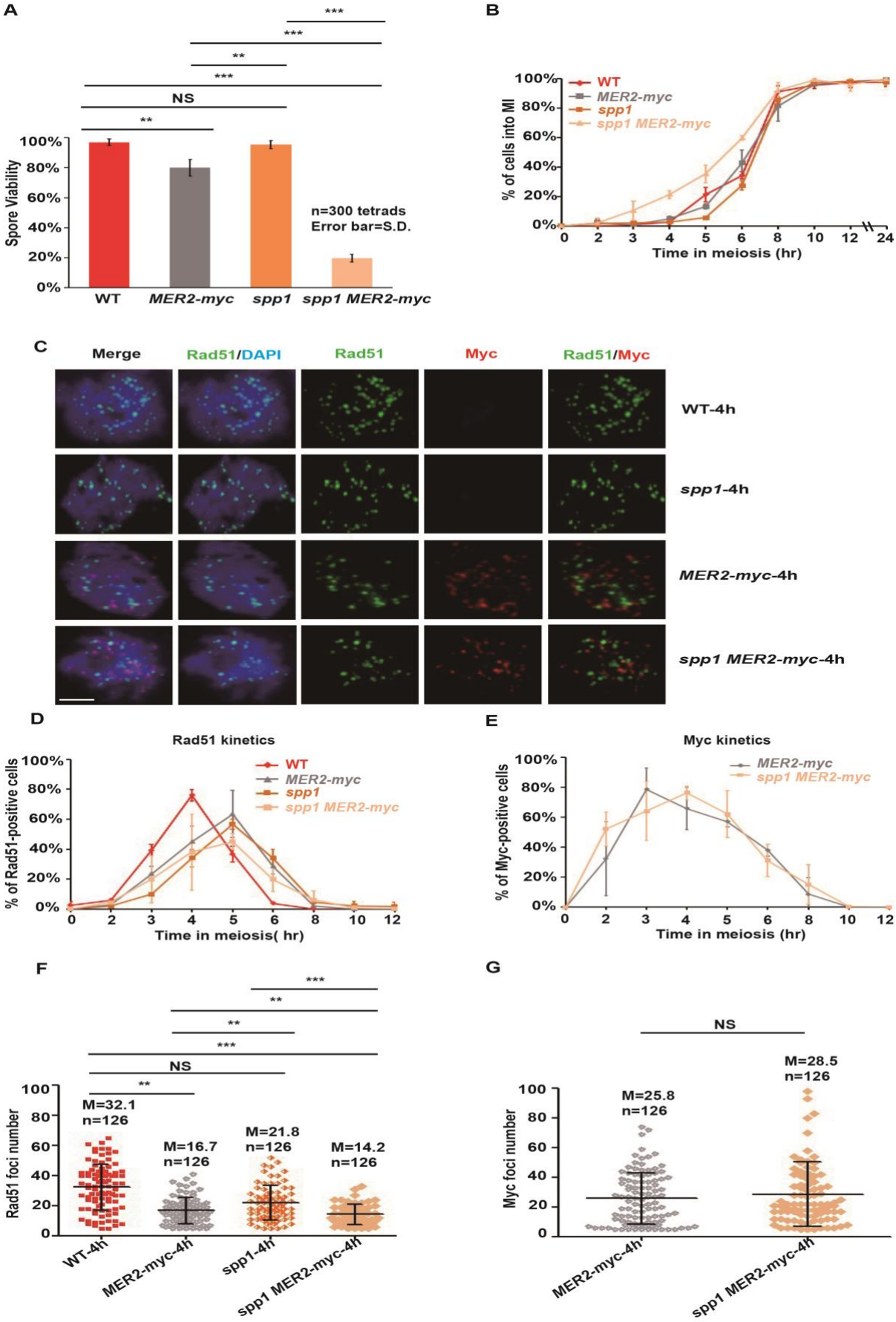
A
***
***
**
***
NS
**
Spore Viability
100%
80%
60%
40%
20%
0%
n=300 tetrads
Error bar=S.D.
WT
MER2-myc
spp1
spp1 MER2-myc
B
% of cells into MI
WT
MER2-myc
spp1
spp1 MER2-myc
Time in meiosis (hr)
C
Merge
Rad51/DAPI
Rad51
Myc
Rad51/Myc
WT-4h
spp1-4h
MER2-myc-4h
spp1 MER2-myc-4h
D
Rad51 kinetics
% of Rad51-positive cells
Time in meiosis(hr)
E
Myc kinetics
% of Myc-positive cells
Time in meiosis (hr)
F
Rad51 foci number
M=32.1
n=126
M=16.7
n=126
M=21.8
n=126
M=14.2
n=126
WT-4h
MER2-myc-4h
spp1-4h
spp1 MER2-myc-4h
G
NS
Myc foci number
M=25.8
n=126
M=28.5
n=126
MER2-myc-4h
spp1 MER2-myc-4h

Figure 6. *spp1* does not show a synthetic interaction with *MER2-myc* in Rad51 focus formation.

(A). Spore viability analysis of the wild-type (ZYY1028), *spp1* (ZYY892), *MER2-myc* (ZYY893), and *spp1 MER2-myc* (ZYY1030) strains. Three hundred tetrads were counted for each independent analysis. Each error bar indicates standard deviation (S.D.) on basis of three independent experiments. * $p<0.05$; ** $p<0.01$; *** $p<0.001$. NS indicates not significant. The data were analyzed by the Wilcoxon Mann-Whitney *U* test.

(B). DAPI staining analysis of each strain. One hundred cells were randomly counted at each time point. Each plotted value represents the mean value ± standard deviation (S.D.) based on three independent time courses. A parallel slash indicates a period from 12 hr to 24 hr.

(C). Cytology immunostaining of Rad51 (green), myc (red), and DAPI (blue). The bar indicates two micrometers.

(D). Kinetics of Rad51-positive cells. One hundred cells were randomly counted in three independent experiments. Each plotted value represents the mean value ± standard deviation (S.D.).

(E). Kinetics of myc-positive cells. A total of 100 cells were randomly counted in three independent experiments. Each plotted value represents the mean value ± standard deviation (S.D.) based on three independent time courses.

(F). Number of Rad51 foci. Forty-two cells were randomly counted in each of three independent experiments (n=126; 42x3). The black line indicates the mean value ± standard deviation (S.D.) of 126 cells. * $p<0.05$; ** $p<0.01$; *** $p<0.001$. NS indicates not significant. The data were analyzed by The Wilcoxon-Mann-Whitney *U* test.

(G). A number of myc foci. Forty-two cells were randomly counted in each of three independent experiments (n=126; 42x3). The black line indicates the mean value ± standard deviation (S.D.) of 126 cells. * $p<0.05$; ** $p<0.01$; *** $p<0.001$. NS indicates not significant. The data were analyzed by the Wilcoxon-Mann-Whitney *U* test.

3-7. The *rtf1* deletion shows a weak genetic interaction with *SPO11-FLAG* in DSB formation.

Rtf1 genetically interacts with the RMM complex, which recruits the Spo11 complex for DSB formation [76]. Hence, to determine whether there is an interaction between *rtf1* and *SPO11*, I analyzed the double mutant allele strain of *rtf1 SPO11-FLAG*. The N-terminal and C-terminal of Spo11 are essential for the protein's function, possibly for interaction with other meiotic DSB enzymes [77]. A previous study showed that the Spo11-Flag exhibits an altered activity when combined with a weak Spo11 mutant [78]. As reported [79], the spore viability of *SPO11-FLAG* cells was 98.8 ± 1.2%. In the *rtf1 SPO11-FLAG* strain, the spore viability was 80.7 ± 6.7%, which was similar to that of the *rtf1* control mutant (Fig. 7 A). This finding indicates that there was little genetic interaction between *rtf1* and *SPO11-FLAG* in spore viability. DAPI analysis showed that *rtf1 SPO11-FLAG* cells enter MI at 5.5 hr, which is delayed compared to *SPO11-FLAG* and wild-type control, but slightly earlier than the *rtf1* mutant (Fig. 7 B).

To determine whether *rtf1 SPO11-FLAG* affects the DSB formation, I analyzed the Rad51 focus formation in the *rtf1 SPO11-FLAG* strain during the meiosis time course. The Rad51 focus-positive cells in the *SPO11-FLAG* strain peaked at 5 hr with 62.1 ± 9.8%, and in the *rtf1 SPO11-FLAG* strain, it was 73.3 ± 5.2% (Fig. 7 C, D). In the *SPO11-FLAG* strain, the mean value of Rad51-positive focus number per positive nucleus was 29.1 ± 16.5, which is similar to that in wild-type. The *rtf1 SPO11-FLAG* strain showed 25.2 ± 16.0, which is comparable to that in the *rtf1* mutant (Fig. 7 E). These results indicate the tag addition does not affect the function of Spo11 in DSB formation, particularly in the *rtf1* mutant, indicating there is little genetic interaction between *rtf1* and *SPO11-FLAG* in DSB formation.

Figure 7

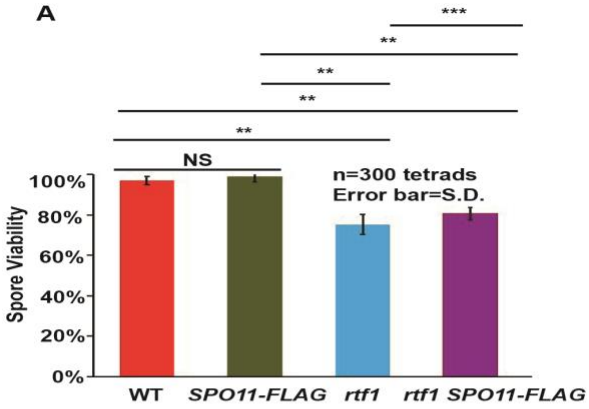
A
***
**
**
**
**
NS
n=300 tetrads
Error bar=S.D.
Spore Viability
100%
80%
60%
40%
20%
0%
WT
SPO11-FLAG
rtf1
rtf1 SPO11-FLAG

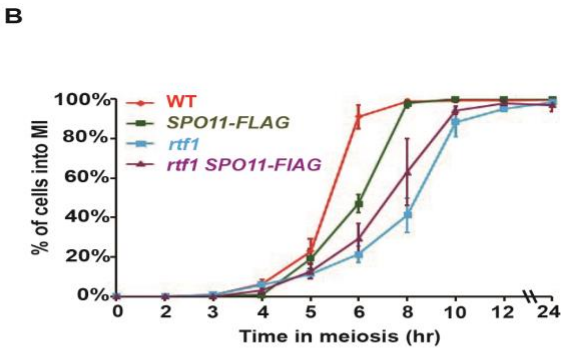
B
% of cells into MI
100%
80%
60%
40%
20%
0%
WT
SPO11-FLAG
rtf1
rtf1 SPO11-FIAG
0
2
3
4
5
6
8
10
12
24
Time in meiosis (hr)

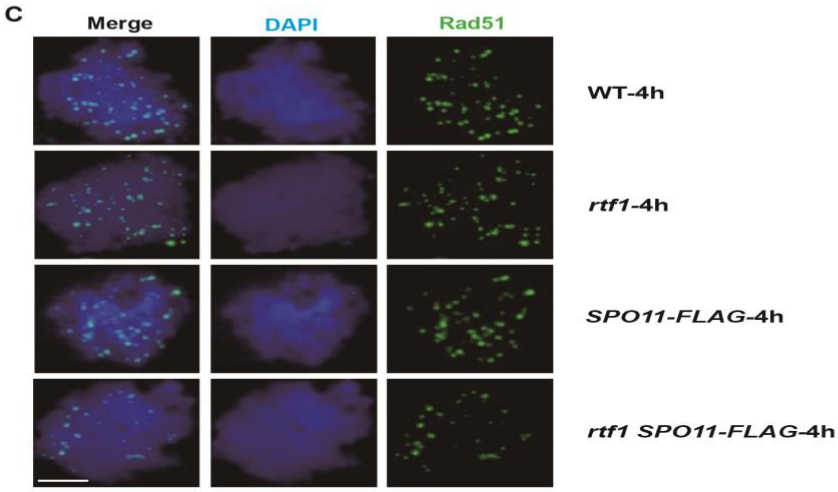
C
Merge
DAPI
Rad51
WT-4h
rtf1-4h
SPO11-FLAG-4h
rtf1 SPO11-FLAG-4h

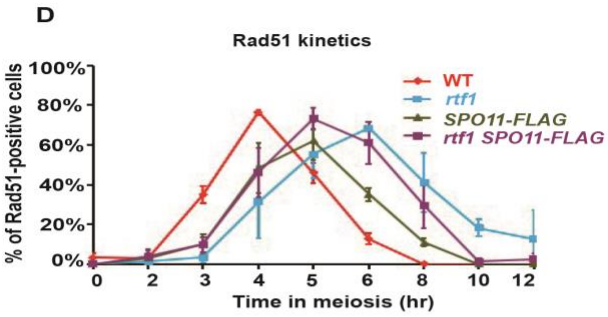
D
Rad51 kinetics
% of Rad51-positive cells
100%
80%
60%
40%
20%
0%
WT
rtf1
SPO11-FLAG
rtf1 SPO11-FLAG
0
2
3
4
5
6
8
10
12
Time in meiosis (hr)

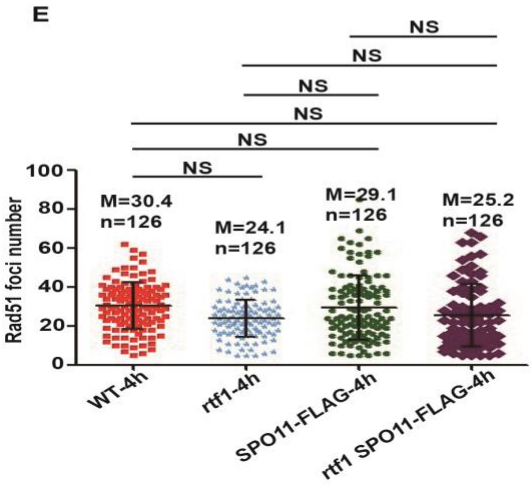
E
NS
NS
NS
NS
NS
NS
Rad51 foci number
100
80
60
40
20
0
M=30.4
n=126
M=24.1
n=126
M=29.1
n=126
M=25.2
n=126
WT-4h
rtf1-4h
SPO11-FLAG-4h
rtf1 SPO11-FLAG-4h

Figure 7. The *rtf1* deletion does not have a genetic interaction with *SPO11-FLAG* in Rad51 focus formation.

(A). Spore viability analysis of the wild-type (ZYY1028), *rtf1* (ZYY389), *SPO11-FLAG* (ZYY1031), and *rtf1 SPO11-FLAG* (ZYY1032) strains. Three hundred tetrads were counted for each independent analysis. Each error bar indicates standard deviation (S.D.) on basis of three independent experiments. * $p<0.05$; ** $p<0.01$; *** $p<0.001$. NS indicates not significant. The data were analyzed by the Wilcoxon Mann-Whitney *U* test.

(B). DAPI staining analysis of each strain. One hundred cells were randomly counted at each time point. Each error bar indicates standard deviation (S.D.) based on three independent time courses. A parallel slash indicates a period from 12 hr to 24 hr.

(C). Cytology immunostaining of Rad51 (green) and DAPI (blue). Rad51 was treated with primary antibody at a 1:200 dilution and secondary antibody at a 1:2000 dilution. The bar indicates two micrometers.

(D). Kinetics of Rad51-positive cells. One hundred cells were randomly counted in three independent experiments. Each plotted value represents the mean value ± standard deviation (S.D.).

(E). Number of Rad51 foci. Forty-two cells were randomly counted in each of three independent experiments (n=126; 42x3). The black line indicates the mean value ± standard deviation (S.D.) of 126 cells. * $p<0.05$; ** $p<0.01$; *** $p<0.001$. NS indicates not significant. The data were analyzed using the Wilcoxon-Mann-Whitney *U* test.

3-8. *rtf1 REC114-myc dmc1* and *spp1 REC114-myc dmc1* form few DSBs in the genome.

The reduction of DSB frequencies could be explained either by reduced DSB frequencies *per se* or by rapid turnover such as rapid DSB repair. *dmc1* deletion resulted in defective homologous recombination or did not form any recombination intermediate turnover, and accumulated DSBs during meiosis [13]. In the strains with a *dmc1* background, it is easy to count the number of Rad51 foci, and calculate the number of DSBs without considering the turnover.

On SPM plates, *rtf1 REC114-myc dmc1* forms only seldom asci after incubation for two days, and the spore viability rarely formed spores in the mutant showed the viability of 0.42 ± 0.9%. On the other hand, *spp1 REC114-myc dmc1* forms more asci with almost 30%, but its spore viability was 0.33 ± 0.88%, indicating that Dmc1 played a critical function in spore viability in either *rtf1 REC114-myc* or *spp1 REC114-myc*.

In this *dmc1* background, I checked the genetic interaction of *REC114-myc* with either *rtf1* or *spp1*. I first performed DAPI staining to analyze the entrance into meiosis I. The results of three independent experiments showed that *dmc1*, *rtf1 dmc1*, *spp1 dmc1,* and *REC114-myc dmc1* maintained prophase I arrest. Importantly, the *rtf1 REC114-myc dmc1* entered MI at 5.5 hr and finished MI at around 10 hr (Fig. 8 A), suggesting few DSBs were induced in this strain. The *spp1 REC114-myc dmc1* cells delay by ~1 hr.

To determine their DSB formation, I used the immuno-staining method for Rad51. In the *dmc1* strain, Rad51 accumulated during the time course without any turnover [13, 80]. Rad51-positive cells in the *dmc1* strain plateaued from 4 hr with 88.3 ± 6.7%. In the *REC114-myc dmc1*, *rtf1 dmc1*, *spp1 dmc1* controls, the number of Rad51-positive cells appeared similarly with that in *dmc1.* Importantly, the *rtf1 REC114-myc dmc1* strain did not form any Rad51 foci, while the *spp1 REC114-myc dmc1* strain formed Rad51 foci (Fig. 8 B, C). In the analysis of Rad51 focus number, at 4 hr, the mean value was 32.3 ± 16.3 in the *dmc1* strain. The *rtf1 dmc1* and *REC114-myc dmc1* strains slightly reduced 26.9 ± 18.1 and 25.0 ± 12.3, respectively, compared to the *dmc1* strain. No focus was seen in the *rtf1 REC114-myc dmc1* strain. On the other hand, the mean value at 6 hr was 33.1 ± 24.5 in the *spp1 dmc1* strain while 26.5 ± 11.6 in the *spp1 REC114-myc dmc1* strain (Fig. 8 D). These confirmed the above findings that the *rtf1*, but not *spp1* mutations showed genetic interaction with *REC114-*

myc in DSB formation and suggested that the reduction of Rad51 foci in *rtf1 Rec114-myc* is not due to rapid repairing of DSB formation.

Figure 8

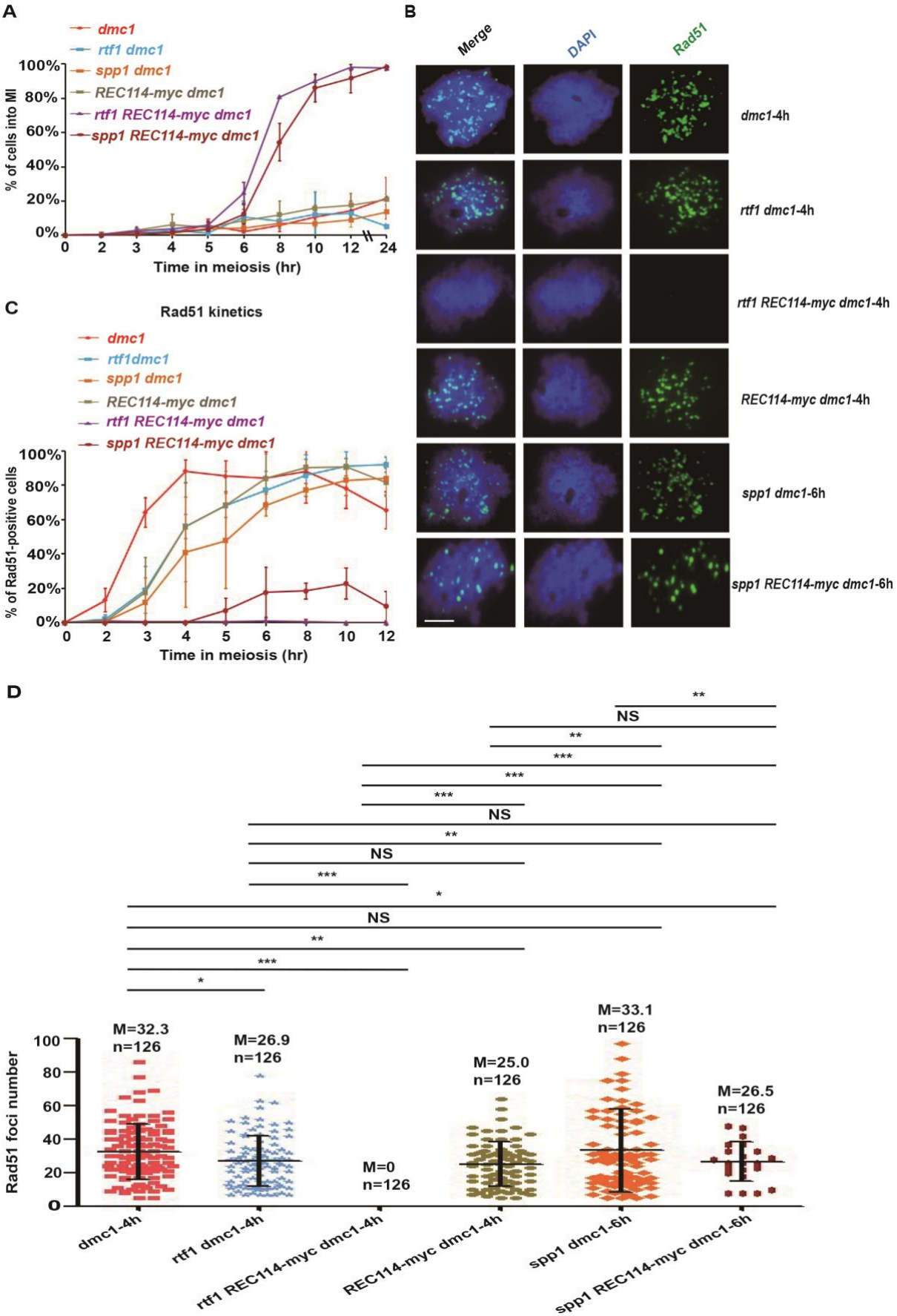
A
dmc1
rtf1 dmc1
spp1 dmc1
REC114-myc dmc1
rtf1 REC114-myc dmc1
spp1 REC114-myc dmc1
% of cells into MI
Time in meiosis (hr)
B
Merge
DAPI
Rad51
dmc1-4h
rtf1 dmc1-4h
rtf1 REC114-myc dmc1-4h
REC114-myc dmc1-4h
spp1 dmc1-6h
spp1 REC114-myc dmc1-6h
C
Rad51 kinetics
% of Rad51-positive cells
Time in meiosis (hr)
D
Rad51 foci number
M=32.3 n=126
M=26.9 n=126
M=0 n=126
M=25.0 n=126
M=33.1 n=126
M=26.5 n=126
NS
dmc1-4h
rtf1 dmc1-4h
rtf1 REC114-myc dmc1-4h
REC114-myc dmc1-4h
spp1 dmc1-6h
spp1 REC114-myc dmc1-6h

Figure 8. *rtf1* and *spp1* show synthetic defects with *REC114-myc* in Rad51 focus formation in the strains with a *dmc1* background.

(A). DAPI staining analysis of the *dmc1* (ZYY999), *rtf1 dmc1* (ZYY997), *REC114-myc dmc1* (ZYY1139), *rtf1 REC114-myc dmc1* (ZYY1029), *spp1 dmc1* (ZYY1148), and *spp1 REC114-myc dmc1* (ZYY1151) strains. One hundred cells were randomly counted at each time point. Each error bar indicates standard deviation (S.D.) based on three independent time courses. A parallel slash indicates a period from 12 hr to 24 hr.

(B). Cytology immunostaining of Rad51 (green) and DAPI (blue). Rad51 was diluted with primary antibody at a 1:200 dilution and secondary antibody at a 1:2000 dilution. The bar indicates two micrometers.

(C). Kinetics of Rad51-positive cells. One hundred cells were randomly counted in three independent experiments. Each error bar indicates standard deviation (S.D.) based on three independent time courses.

(D). Number of Rad51 foci. Forty-two cells were randomly counted in each of three independent experiments (n=126; 42x3). The black lines indicate the mean value ± standard deviation (S.D.) of 126 cells. * $p<0.05$; ** $p<0.01$; *** $p<0.001$. NS indicates not significant. The data were analyzed by the Wilcoxon Mann-Whitney *U* test.

3-9. *rtf1 MER2-myc dmc1* and *spp1 MER2-myc dmc1* form few DSBs in the genome.

I also extended to the genetic interactions between histone modification machinery and the *MER2-myc* allele in the *dmc1* background. Similar to the *rtf1 REC114-myc dmc1* and *spp1 REC114-myc dmc1* strains, the *rtf1 MER2-myc dmc1* strain entered meiosis I at 4.5 hr and finished meiosis progression at around 10 hr. The *spp1 MER2-myc dmc1* strain entered meiosis I at 6 hr (Fig. 9 A). The spore viability of *rtf1 MER2-myc dmc1* and *spp1 MER2-myc dmc1* is nearly 0%.

In the kinetic analysis of Rad51-positive cells, the *rtf1 MER2-myc dmc1* strain showed few Rad51-positive cells. In the *spp1 MER2-myc dmc1* strain, Rad51-positive cells reached to 34.6 ± 30.0% (Fig. 9 B, C). In the analysis of Rad51 focus number, at 4 hr, in the *rtf1 MER2-myc dmc1* and *spp1 MER2-myc dmc1* strains, the mean values were 6.0 and 26.2 ± 15.7, respectively (Fig. 9 D). This again supports the finding that strong synthetic interaction of *MER2-myc* occurs with the *rtf1* but not with *spp1*, suggesting that the genetic interaction between histone modification machinery and RMM is independent of loop-tethering to the axis.

Reduction of Rad51 foci not only in *DMC1* but also in *dmc1* background suggests that the genes involved in histone modification machinery have strong genetic interaction with DSB proteins in DSB formation during meiosis in budding yeast.

Figure 9

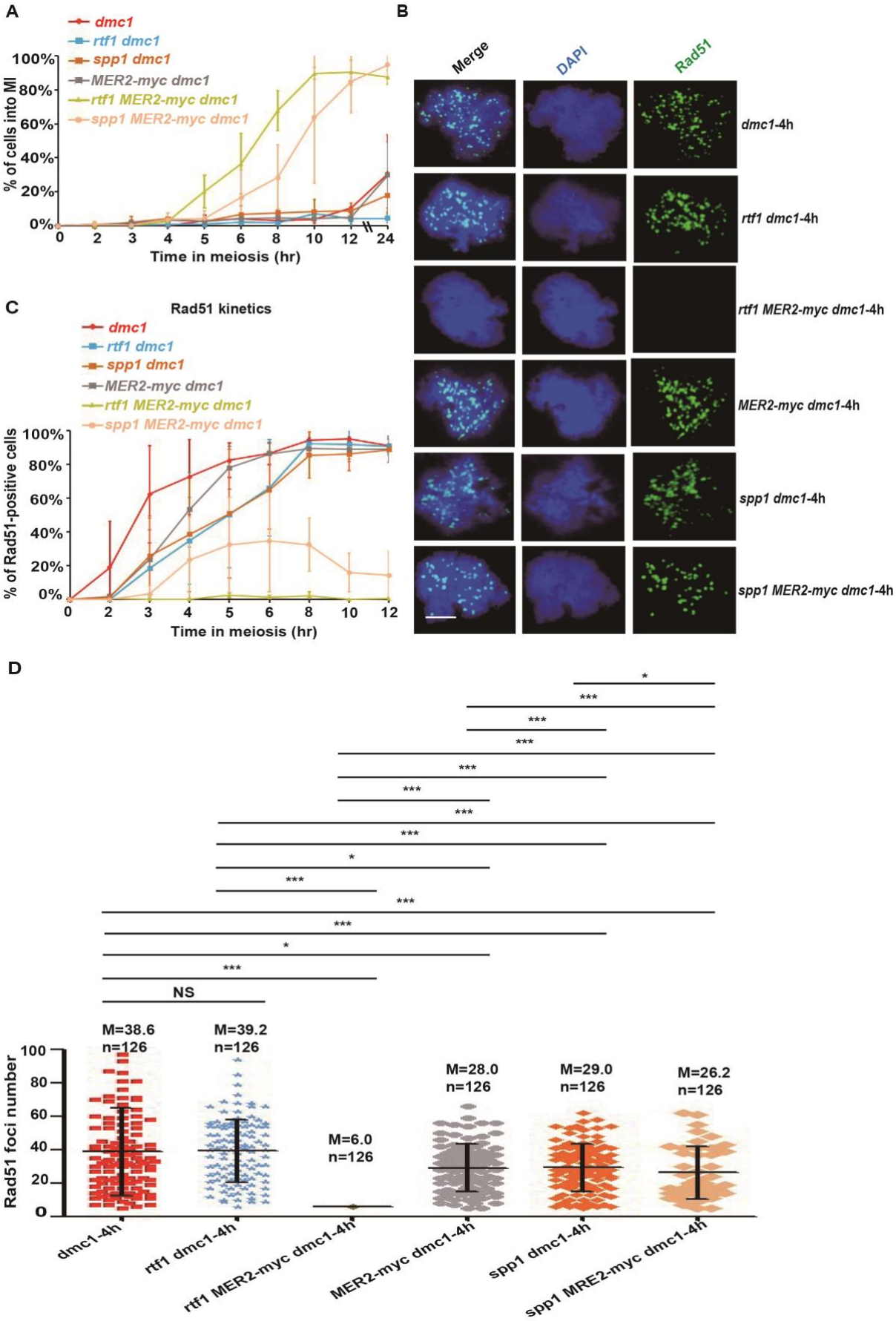
A
dmc1
rtf1 dmc1
spp1 dmc1
MER2-myc dmc1
rtf1 MER2-myc dmc1
spp1 MER2-myc dmc1
% of cells into MI
Time in meiosis (hr)
B
Merge
DAPI
Rad51
dmc1-4h
rtf1 dmc1-4h
rtf1 MER2-myc dmc1-4h
MER2-myc dmc1-4h
spp1 dmc1-4h
spp1 MER2-myc dmc1-4h
C
Rad51 kinetics
% of Rad51-positive cells
Time in meiosis (hr)
D
NS
Rad51 foci number
M=38.6 n=126
M=39.2 n=126
M=6.0 n=126
M=28.0 n=126
M=29.0 n=126
M=26.2 n=126
dmc1-4h
rtf1 dmc1-4h
rtf1 MER2-myc dmc1-4h
MER2-myc dmc1-4h
spp1 dmc1-4h
spp1 MRE2-myc dmc1-4h

Figure 9. *rtf1* and *spp1* show synthetic defects with *MER2-myc* in Rad51 focus formation in the *dmc1* background.

(A). DAPI staining analysis of *dmc1* (ZYY999), *rtf1 dmc1* (ZYY997), *MER2-myc dmc1* (ZYY1142), *rtf1 MER2-myc dmc1* (ZYY1136), *spp1 dmc1* (ZYY1148), and *spp1 MER2-myc dmc1* (ZYY1098) cells. One hundred cells were randomly counted at each time point. Each error bar indicates standard deviation (S.D.) based on three independent time courses. The parallel slash indicates a period from 12 hr to 24 hr.

(B). Cytology immunostaining of Rad51 (green) and DAPI (blue). Rad51 was treated with primary antibody at a 1:200 dilution and secondary antibody at a 1:2000 dilution. The bar indicates two micrometers.

(C). Kinetics of Rad51 positive cells. One hundred cells were randomly counted in three independent experiments. Each error bar indicates standard deviation (S.D.) based on three independent time courses.

(D). Number of Rad51 foci. Forty-two cells were randomly counted in each of three independent experiments (n=126; 42x3). The black lines indicate the mean value ± standard deviation (S.D.) in 126 cells. * $p<0.05$; ** $p<0.01$; *** $p<0.001$. NS means Not Significant. Data were analyzed using the Wilcoxon-Mann-Whitney *U* test.

3-10. Western blot analysis of histone modification.

The results of the analysis of *spp1* deletion strongly excluded a possible role of loop tethering in the genetic interaction between the histone modification machinery and the RMM complex. I confirmed this finding by performing western blotting to examine the histone modification levels in the different mutants assessed in this study, specifically in meiosis. First, the methylation of histones in each strain was analyzed using anti-H3K4me, anti-H3K4me2, anti-H3K4me3, and anti-H3K79me3 antibodies. In wild-type and *REC114-myc* cells, there were identifiable bands obtained at 0 hr and 4 hr with each histone methylation antibody. There is little difference between 0 and 4 hr, indicating persistent histone H3 methylation at lysine K4 and K79 during meiosis. Importantly, for the *rtf1* single mutant and *rtf1 REC114-myc* cells as well as *rtf1 MER2-myc* cells, no bands in H3K4 and H3K79 methylation were observed at either 0 hr or 4 hr, indicating that Rtf1 is essential for both methylations not only in mitotic cells [81] but also in meiotic cells. In *set1* and *set1 REC114-myc* cells, there were no bands in H3K4 methylation but clear bands in H3K79 trimethylation, confirming that Set1 is important for the methylation of H3K4 but is not critical for H3K79 methylation [82]. In *spp1*, *spp1 REC114-myc*, and *spp1 MER2-myc* cells, amounts of H3K4me2 and H3K4me3 were similar with those in the controls, but the bands representing H3K4me were weaker than the controls by about one-half, indicating that Spp1 specifically plays a role in the mono-methylation of H3K4 at enhancer (Fig. 10 A, B).

To confirm the meiosis progression in each strain, anti-Rec8 and anti-Cdc5 antibodies were used in this analysis. Rec8 is a meiosis-specific gene encoding a subunit of a meiosis-specific subunit of cohesin complex, which is a good marker for entrance into meiosis progression [83]. Cdc5 (polo-like kinase) is the gene that is a marker of the exit from the mid-pachytene stage [15]. The levels of Rec8 indicated that the wild-type cells induced Rec8 expression after 2 hr and decreased from 8 hr. The *REC114-myc* cells showed similar expression of Rec8 to wild-type. The *rtf1* and *rtf1 REC114-myc* cells showed Rec8 expression after 2 hr and delayed the disappearance by 12 hr. In the *spp1* strain, Rec8 expression started at 3 hr and diminished at 10 hr. The *spp1 REC114-myc* strain induced Rec8 from 2 hr and showed ~2 hr delay in its disappearance relative to the *spp1*. The *MER2-myc* and the *rtf1 MER2-myc* cells showed Rec8 expression from 2 hr and decreased it at approximately 10 hr. In the

spp1 MER2-myc strains, Rec8 was induced at 2 hr and repressed at approximately 10 hr.

The levels of Cdc5 indicated that the wild-type cell induced Cdc5 between 5 hr and 6 hr (exit from the mid-pachytene stage), and reduced between 8 hr and 10 hr (exit of MI). The *REC114-myc* cells exited mid-pachytene at 8 hr with concomitant delay in the disappearance from 10 hr. In the *rtf1* and *rtf1 REC114-myc* strains, the cells exited the mid-pachytene meiotic stage between 8 hr and 12 hr, and the highest band density of Cdc5 was observed at 10 hr. In the *spp1* strain, the cells exited the mid-pachytene meiotic stage between 6 hr and 8 hr, and the highest band intensity was observed at 8 hr. In the *spp1 REC114-myc* strain, the cells exited the mid-pachytene meiotic stage between 6 hr and 12 hr and showed constant Cdc5 band intensity. The *MER2-myc* cells induced the Cdc5 expression between 8 hr and 10 hr and disappeared from 10 hr. In the *rtf1 MER2-myc* strain, Cdc5 increased between 6 hr and 12 hr without disappearance. The *spp1 MER2-myc* cells increased Cdc5 between 5 hr and 8 hr, after that became disappeared (Fig. 10 D).

I also check the histone modification status in the different strains with a *dmc1* background. In this study, I examined only H3K4me3 trimethylation. The *dmc1*, *rtf1 dmc1*, *REC114-myc dmc1*, *spp1 dmc1*, and *MER2-myc dmc1* cells displayed clear H3K4me3 bands of similar density between 0 hr and 4 hr. The *rtf1 REC114-myc dmc1* and *rtf1 MER2-myc dmc1* cells did not show any band at 0 hr and 4 hr. The *spp1 REC114-myc dmc1* and *spp1 MER2-myc dmc1* cells both showed a weak band of methylation at 0 hr and 4 hr relative to the *dmc1* control (Fig. 10 C). These confirmed the methylation status is similar between wild-type and *dmc1* backgrounds.

Western blotting of Rec8 and Cdc5 showed that the *dmc1*, *rtf1 dmc1*, *REC114-myc dmc1*, *spp1 dmc1*, and *MER2-myc dmc1* cells induced Rec8 at 2 hr and accumulated through the 12th hr without any disappearance, indicating an arrest in meiosis. Consistent with this, the evaluation of the Cdc5 band failed to detect Cdc5 expression. In *rtf1 REC114-myc dmc1*, *spp1 REC114-myc, rtf1 MER2-myc dmc1,* and *spp1 MER2-myc dmc1* cells all induced Rec8 expression at 2 hr with the accumulation of the protein. On the other hand, the *rtf1 MER2-myc dmc1* strain did show the disappearance of Rec8 at approximately 10 hr, indicating the pachytene exit in the cell. The *spp1 MER2-myc dmc1* cells decreased Rec8 levels approximately at 12 hr. The Cdc5 western confirmed an arrest at the mid-pachytene stage in the *dmc1*, *rtf1 dmc1*, *REC114-myc dmc1*, *spp1 dmc1*, and *MER2-myc dmc1* cells without any expression

of Cdc5. The *rtf1 MER2-myc dmc1* cells showed the expression of Cdc5 from 5 hr and decreased the expression from 10 hr, indicating the exit from mid-pachytene stage. The *spp1 MER2-myc dmc1* cells expressed Cdc5 between 5 hr and 12 hr without decreased expression (Fig. 10 E), indicating there is an arrest in MI.

Figure 10

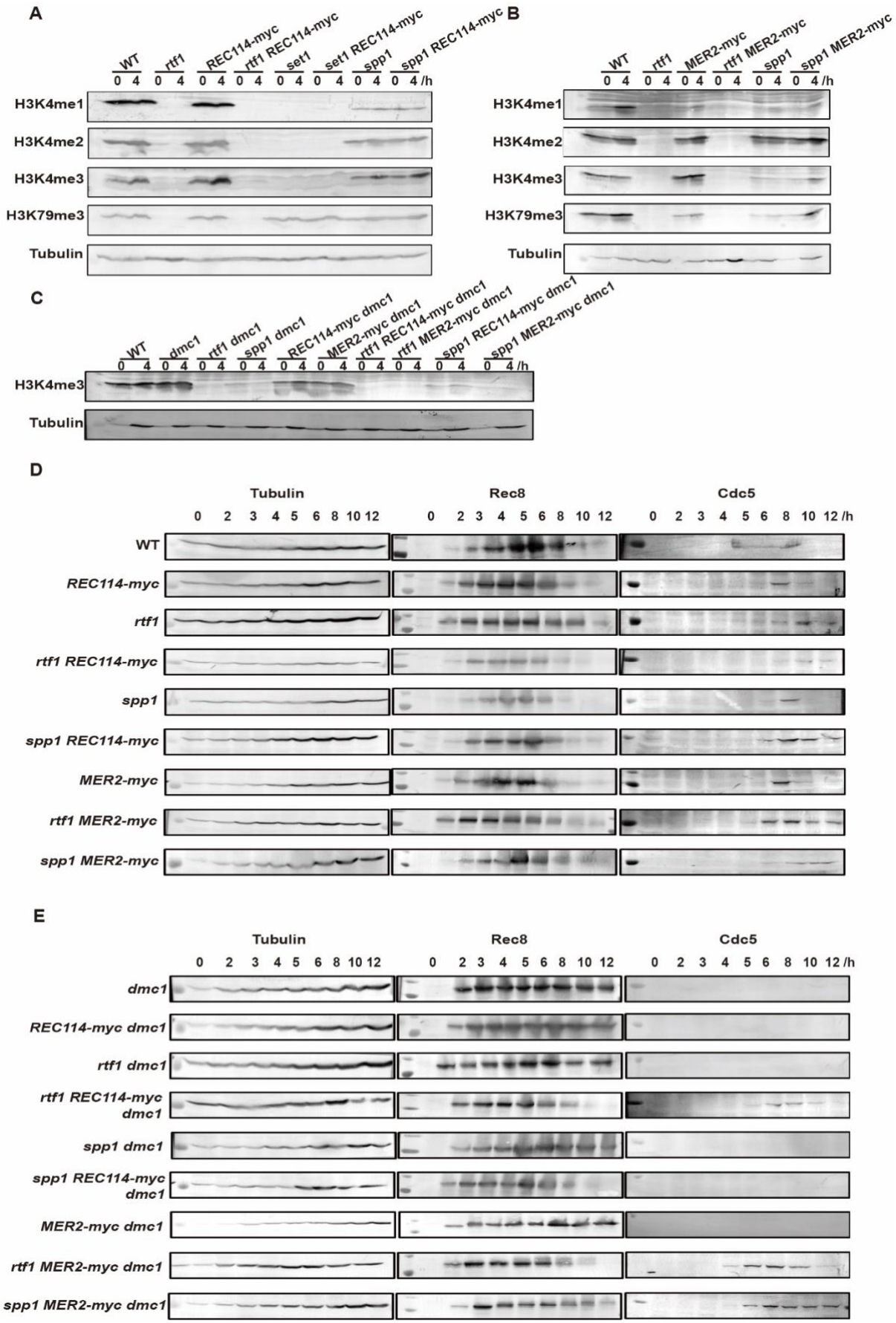
A
WT
rtf1
REC114-myc
rtf1 REC114-myc
set1
set1 REC114-myc
spp1
spp1 REC114-myc
0 4 0 4 0 4 0 4 0 4 0 4 0 4 0 4 /h
H3K4me1
H3K4me2
H3K4me3
H3K79me3
Tubulin
B
WT
rtf1
MER2-myc
rtf1 MER2-myc
spp1
spp1 MER2-myc
0 4 0 4 0 4 0 4 0 4 0 4 /h
H3K4me1
H3K4me2
H3K4me3
H3K79me3
Tubulin
C
WT
dmc1
rtf1 dmc1
spp1 dmc1
REC114-myc dmc1
MER2-myc dmc1
rtf1 REC114-myc dmc1
rtf1 MER2-myc dmc1
spp1 REC114-myc dmc1
spp1 MER2-myc dmc1
0 4 0 4 0 4 0 4 0 4 0 4 0 4 0 4 0 4 0 4 /h
H3K4me3
Tubulin
D
Tubulin
Rec8
Cdc5
0 2 3 4 5 6 8 10 12 /h
WT
REC114-myc
rtf1
rtf1 REC114-myc
spp1
spp1 REC114-myc
MER2-myc
rtf1 MER2-myc
spp1 MER2-myc
E
Tubulin
Rec8
Cdc5
0 2 3 4 5 6 8 10 12 /h
dmc1
REC114-myc dmc1
rtf1 dmc1
rtf1 REC114-myc dmc1
spp1 dmc1
spp1 REC114-myc dmc1
MER2-myc dmc1
rtf1 MER2-myc dmc1
spp1 MER2-myc dmc1

Figure 10. Western blot of each strain confirms the results.

(A). Western blot of *REC114-myc* strains with anti-H3K4me, anti-H3K4me2, anti-H3K4me3, and anti-H3K79me3 antibodies, with anti-tubulin antibody as the control.

(B). Western blot of the strains expressing *MER2-myc* using anti-H3K4me, anti-H3K4me2, anti-H3K4me3, and anti-H3K79me3 antibodies, with anti-tubulin antibody as the control.

(C). Western blot of strains with a *dmc1* background using anti-H3K4me3 with anti-tubulin antibody as the control.

(D). Western blot of all strains with a MSY background using anti-Rec8 and anti-Cdc5 antibodies with anti-tubulin antibody as the control.

(E). Western blot of all strains with a *dmc1* background using anti-Rec8 and anti-Cdc5 antibodies with anti-tubulin antibodies as the control.

Chapter IV. Discussion

The multiple situations of spore viability, kinetics of Rad51 positive cells and Rad51 focus formation per nucleus in different stains during meiosis.

The spore viability indicates the importance of genes during meiosis. The mutations such as *rtf1*, *cdc73*, *set1,* or *spp1* single mutants showed a reduced level of spore viability indicating the different important roles during meiosis. *rtf1 REC114-myc*, *rtf1 MER2-myc*, *cdc73 REC114-myc* showed strong synthetic defects in spore viability. And the defects in the checking of their Rad51 focus formation reflected those synthetic defections. *rtf1 MER2-myc* showed less spore viability than that in *rtf1 REC114-myc,* indicating a stronger synergistic effect between *rtf1* and *MER2-myc* during meiosis. *rtf1 MER2-myc* shows more frequency of Rad51 positive cells and also the focus number per nucleus, indicates its fewer DSB formation is probably caused by the different process of DSB repairing intermediates such as crossover formation. The spore viability of *set1 REC114-myc* is higher than that in *rtf1* and *cdc73* combination alleles with *REC114-myc*, might be caused by randomly separation of homologous chromosomes during meiosis. The results of the Rad51 foci formation in *cdc73 REC114-myc* and *rtf1 REC114-myc* strains were the same: no DSB, explaining the strong synthetic defects seen in spore viability. However, when the cells of *cdc73 REC114-myc* were induced in the SPM plate, the shape of spores showed large oval, instead of round as other strains. This high spore viability of 61.4% in SPM plates might due to the sensitivity of spore membrane to osmotic stress.

The single PAF1C might interact with RMM complex for meiotic DSB formation.

In yeast, the PAF1C regulates the mono-ubiquitination of histone H2B. Set1 and Dot1 histone modification transferases methylate H3K4 and H3K79, respectively for DSB formation [64, 84]. In this study, the homozygous combination strains of *rtf1* with myc-tagged versions of *REC114* and *MER2* showed a certain number of Rad51 foci, suggesting a strong genetic interaction between *rtf1* and *REC114-myc* or *MER2-myc* during DSB formation. The distribution pattern of DSB formation in the *rtf1* strain differed from that in the *set1* or *set1dot1* strain [58], indicating histone modification independent way of Rtf1 for Meiotic DSB formation. Genome-wide ssDNA mapping identified 134 hotspots with substantially increased DSB activities in the *rtf1* strain, suggesting the repressive role of Rtf1 or PAF1C during DSB formation in a region-

specific manner [58]. Therefore, PAF1C has the possibility to ubiquitinate RMM for meiotic DSB formation.

Spp1 in Set1C/COMPASS is unique for the loop-axis tethering to produce DSBs. Spp1 is a subunit of Set1C/COMPASS that is a key regulator of H3K4 trimethylation. Among the components of Set1C/COMPASS, SWD1, SWD3, and SET1 constitute a core of the complex, and the absence of any of these subunits abolishes methylation of lysine 4 on histone H3. The Swd1, Swd3, Bre2, and Sdc1 form a small complex to interact with the SET domain, while none of these proteins alone can interact with Set1 suggesting that subunit interactions are required for these four proteins to bind the SET domain. Spp1 indirectly interacts with the SET domain through Swd3 to alter the catalytic pocket of Set1 that allows the trimethylation of H3K4. Swd2 interacts with the N-terminal of Set1, and its ubiquitynation at K68, 69 sites facilities the recruitment of Spp1 and H3K4me3. Shg1 interacts with another motif of Set1. Spp1 has a PHD domain to recognize dimethylation and trimethylation of H3K4 on chromatin loops, and the C-terminal of Spp1 interacts with Mer2 on chromosome axis. With the N-terminal and C-terminal binding with two different proteins on the chromatin loop and chromosome axis respectively, the loop tethers to the axis. Based on above, Spp1 subunit should be the only essential protein as a bridge protein for loop-axis tethering and disrupting the Spp1-Set1 interaction mildly decreases H3K4me3 levels and does not affect meiotic recombination initiation [85].

The loop-axis tethering independent pathway is productive to generate DSBs. Spp1 interacts with H3K4me3 and Mer2 to activate the loop-axis tethering, then allowing subsequent DNA cleavage by Spo11 [86]. Analysis of Rad51 focus formation in the homozygous strains of *spp1 REC114-myc* and *spp1 MER2-myc* showed that the number of DSBs in a nucleus was slightly reduced in the delayed meiosis progression, while other combinations between histone modification proteins and RMM all largely decreased DSBs' number. This indicates that in the absence of Spp1, which encodes a key component of loop-axis tethering, there is another productive pathway substantially contributes to DSB formation.

PAF1C and Set1/COMPASS histone modification machinery associates with the chromosome axis protein RMM for meiotic DSB formation. It has been reported that there was one non-histone methylation target of the histone modification machinery,

the Dam1, which is involved in microtubule dynamics at kinetochores, [87]. Therefore, the histone modification machinery through Paf1C and Set1 might methylate RMM on the chromosome axis as a non-histone target to produce DSBs (Fig 11. Model). This hypothesis requires additional checking for the status of various proteins in histone modification machinery and may contributes one more possibility for analyzing cancer and Parkinson's diseases.

The C-terminal of Rec114 and Mer2 is important for their functions in meiotic DSB formation.

In the hypomorphic alleles of *REC114* and *MER2*, DSB frequencies are moderately decreased, while combined with the mutations of *rtf1* or *cdc73* subunits in PAF1C and *set1*, they showed severe synthetic defects on DSB formation. This suggests that the C-terminal of Rec114 and Mer2 are essential for their functions in meiotic DSB formation, and the addition of myc-tag might alter the chromosome structure which is interesting for further analysis.

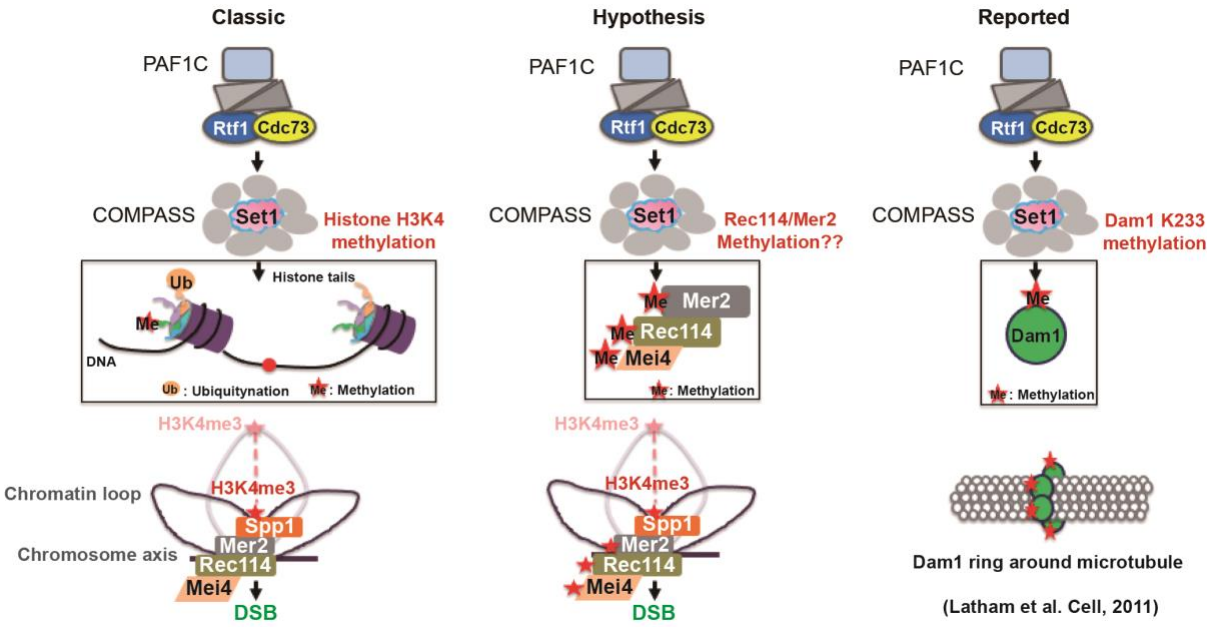

Figure 11. Model.

Previous studies showed the histone modification machinery including PAF1C and Set1 trimethylate H3K4 on the chromosome loop. Spp1 reads both H3K4me3 and Mer2 from the loop to the axis. Mer2 recruits Spo11 to produce DSBs. Previous studies demonstrated non-histone target of Set1, which was Dam1. Dam1 forms a ring structure around microtubules for proper chromosome segregation. This Dam1 methylation by Set1 also requires PAF1C. Based on this, I propose that there are other non-histone target by Set1, which could be a component of RMM such as Rec114 or Mer2 or others. The Set1 activity for these histone targets is also regulated by PAF1C as seen for H3 methylation.

Acknowledgments

I appreciate Prof. Akira Shinohara and Prof. Miki Shinohara for helpful suggestions for completing the research. I thank all lab members, who made nice environment during this period. And I also appreciate the ideas from Prof. Susan M Gasser and Prof. Neil Hunter.

Table1. Strains list

MSY831/833: *MATα/a, ho::LYS2, lys2, ura3, leu2::hisG, trp1::hisG*
NKY1551:*MATα/a,ho::LYS2,lys2,leu2::hisG,ura3,His4X-LEU2(BamH1)-URA3/his4B-LEU2(Mlu1), arg4-bgl/arg4-nsp*
ZYY389: MSY831/833 with *rtf1::TRP1*
ZYY391: MSY831/833 with rtf1::TRP1, T*RP1, REC114-9myc:: kanMX6*
ZYY411: MSY831/833 with *REC114-9myc:: kanMX6*
ZYY733: MSY831/833 with *set1::URA3*
ZYY736: MSY831/833 with *cdc73::TRP1, TRP1, REC114-9myc:: kanMX6*
ZYY739: MSY831/833 with *spp1::HYG, REC114-9myc:: kanMX6*
ZYY811: MSY831/833 with *cdc73::TRP1, TRP1*
ZYY812: MSY831/833 with *set1:: URA3,REC114-9myc:: kanMX6*
ZYY874: MSY831/833 with *rtf1::TRP1, TRP1, Mer2-13myc:: TRP1*
ZYY892: MSY831/833 with *spp1::HYG*
ZYY893: MSY831/833 with *Mer2-13myc::TRP1*
ZYY997: NKY1551 with *rtf1::TRP1, dmc1::URA3*
ZYY999: NKY1551 with *dmc1::URA3*
ZYY1028: MSY831/833
ZYY1029: NKY1551 with *rtf1::TRP1, REC114-9myc:: KANMX, dmc1:: URA3*
ZYY1030: MSY831/833 with *spp1:: HYG, Mer2-13myc::TRP1,TRP1*
ZYY1031: MSY831/833 with *SPO11:: 3FLAG:: kanMX6*
ZYY1032: MSY831/833 with *rtf1::TRP1, SPO11:: 3FLAG:: kanMX6*
ZYY1136: NKY1551 with *rtf1::TRP1, Mer2-13myc::TRP1, dmc1:: URA3*
ZYY1039: NKY1551 with *REC114-9myc:: kanMX6, dmc1:: URA3*
ZYY1142: NKY1551 with *Mer2- 13myc:: TRP1, dmc1:: URA3*
ZYY1148: NKY1551 with *spp1::HYG, dmc1::URA3*
ZYY1151: NKY1551 with *spp1::HYG, REC114-9myc:: kanMX6, dmc1:: URA3*

Legend of the strains list:

ZYY1028, 389, 391, 411, 733, 736, 739, 811, 812, 874, 892, 893,1031,1032 are to check the meiosis progression by DAPI staining, spore viability and kinetics of Rad51 and Myc. NKY1551, ZYY997, 999, 1029, 1098, 1136, 1139, 1142, 1148, 1151 are to do the time course for *dmc1* background strains to analyze the cytology and kinetics of Rad51 staining.

Table2. Dilution of WB antibody

Primary antibody	Secondary antibody
Anti-Tubulin, Serotec, YOL1/34; 1:1000	Anti-Rat-1:7500
Anti-H3K4me, Abcam, Cambridge, ab8895; 1:1000	Anti-Rabbit-1:7500
Anti-H3K4me2, Millipore, Burlington, MA, USA, 07-030; 1:1000	Anti-Rabbit-1:7500
Anti-H3K4me3, Abcam, ab8580;1:1000	Anti-Rabbit-1:7500
Anti-H3K79me3, Abcam, ab2621;1:1000	Anti-Rabbit-1:7500
Anti-Cdc5, SantaCruz, Dallas, TX, USA, sc-33635; 1:200	Anti-Goat-1:7500
Anti-Rec8, raised against guinea pig; 1:200	Anti-Mouse-1:12500
Anti-Myc, Nakarai, Kyoto, Japan, MC045; 1:200	Anti-Mouse-1:7500
Anti-Flag, Invitrogen, MA1-91878-D488; 1:200	Anti-Mouse-1:7500
Anti-Dmc1, raised against rabbit; 1:200	Anti-Rabbit-1:7500

Table3. Dilution of immunostaining chromosome spreads antibody

Primary antibody	Secondary antibody
Anti-Rad51, raised against rabbit; 1:200	Anti-Rabbit-Alexa Fluor-488, Themo Fishers, Waltham, MA, USA; 1:2000
Anti-Myc, Nakarai, Kyoto, Japan, MC045;1:200	Anti-Mouse-Alexa Fluor-594, Themo Fishers, Waltham, MA, USA; 1:2000

References

1. Li, W., et al., *Editorial: Meiosis: From Molecular Basis to Medicine.* Front Cell Dev Biol, 2021. **9**: p. 812292.
2. Duina, A.A., M.E. Miller, and J.B. Keeney, *Budding yeast for budding geneticists: a primer on the Saccharomyces cerevisiae model system.* Genetics, 2014. **197**(1): p. 33-48.
3. Taddei, A. and S.M. Gasser, *Structure and function in the budding yeast nucleus.* Genetics, 2012. **192**(1): p. 107-29.
4. Sou, I.F., et al., *Meiosis initiation: a story of two sexes in all creatures great and small.* Biochem J, 2021. **478**(20): p. 3791-3805.
5. Stahl, F.W., et al., *Does crossover interference count in Saccharomyces cerevisiae?* Genetics, 2004. **168**(1): p. 35-48.
6. Shinohara, M., et al., *Tid1/Rdh54 promotes colocalization of rad51 and dmc1 during meiotic recombination.* Proc Natl Acad Sci U S A, 2000. **97**(20): p. 10814-9.
7. Hinch, A.G., et al., *The Configuration of RPA, RAD51, and DMC1 Binding in Meiosis Reveals the Nature of Critical Recombination Intermediates.* Mol Cell, 2020. **79**(4): p. 689-701 e10.
8. Sasanuma, H., et al., *Remodeling of the Rad51 DNA strand-exchange protein by the Srs2 helicase.* Genetics, 2013. **194**(4): p. 859-72.
9. Shinohara, A., H. Ogawa, and T. Ogawa, *Rad51 protein involved in repair and recombination in S. cerevisiae is a RecA-like protein.* Cell, 1992. **69**(3): p. 457-70.
10. Lee, M.S., et al., *The synaptonemal complex central region modulates crossover pathways and feedback control of meiotic double-strand break formation.* Nucleic Acids Res, 2021. **49**(13): p. 7537-7553.
11. Börner, G.V., N. Kleckner, and N. Hunter, *Crossover/Noncrossover Differentiation, Synaptonemal Complex Formation, and Regulatory Surveillance at the Leptotene/Zygotene Transition of Meiosis.* Cell, 2004. **117**(1): p. 29-45.
12. Zickler, D. and N. Kleckner, *Recombination, Pairing, and Synapsis of Homologs during Meiosis.* Cold Spring Harb Perspect Biol, 2015. **7**(6).
13. Hunter, N. and N. Kleckner, *The single-end invasion: an asymmetric intermediate at the double-strand break to double-holliday junction transition of meiotic recombination.* Cell, 2001. **106**(1): p. 59-70.
14. Hollingsworth, N.M., *Deconstructing meiosis one kinase at a time: polo pushes past pachytene.* Genes Dev, 2008. **22**(19): p. 2596-600.
15. Sourirajan, A. and M. Lichten, *Polo-like kinase Cdc5 drives exit from pachytene during budding yeast meiosis.* Genes Dev, 2008. **22**(19): p. 2627-32.
16. Marston, A.L., *Chromosome segregation in budding yeast: sister chromatid cohesion and related mechanisms.* Genetics, 2014. **196**(1): p. 31-63.
17. Dawson, R.E.M.a.D.S., *Attaching to spindles before they form.* Cell Cycle, 2013. **12**(13): p. 2011–2015.
18. Liu, T. and J. Huang, *DNA End Resection: Facts and Mechanisms.* Genomics Proteomics

Bioinformatics, 2016. **14**(3): p. 126-130.
19. Cloud, V., et al., *Rad51 is an accessory factor for Dmc1-mediated joint molecule formation during meiosis.* Science, 2012. **337**(6099): p. 1222-5.
20. Cooper, T.J., V. Garcia, and M.J. Neale, *Meiotic DSB patterning: A multifaceted process.* Cell Cycle, 2016. **15**(1): p. 13-21.
21. Lam, I. and S. Keeney, *Mechanism and regulation of meiotic recombination initiation.* Cold Spring Harb Perspect Biol, 2014. **7**(1): p. a016634.
22. Schneider, J., et al., *Molecular regulation of histone H3 trimethylation by COMPASS and the regulation of gene expression.* Mol Cell, 2005. **19**(6): p. 849-56.
23. Mersman, D.P., et al., *Charge-based interaction conserved within histone H3 lysine 4 (H3K4) methyltransferase complexes is needed for protein stability, histone methylation, and gene expression.* J Biol Chem, 2012. **287**(4): p. 2652-65.
24. Sharma, A.K. and M.J. Hendzel, *The relationship between histone posttranslational modification and DNA damage signaling and repair.* Int J Radiat Biol, 2019. **95**(4): p. 382-393.
25. Campos, E.I. and D. Reinberg, *Histones: annotating chromatin.* Annu Rev Genet, 2009. **43**: p. 559-99.
26. Xu, Y. and B.D. Price, *Chromatin dynamics and the repair of DNA double strand breaks.* Cell Cycle, 2011. **10**(2): p. 261-7.
27. Rice, J.C. and C.D. Allis, *Histone methylation versus histone acetylation: new insights into epigenetic regulation.* Curr Opin Cell Biol, 2001. **13**(3): p. 263-73.
28. Hayashi, M., et al., *A Conserved Histone H3-H4 Interface Regulates DNA Damage Tolerance and Homologous Recombination during the Recovery from Replication Stress.* Mol Cell Biol, 2021. **41**(4).
29. Thakre, P.K., et al., *Previously uncharacterized amino acid residues in histone H3 and H4 mutants with roles in DNA damage repair response and cellular aging.* FEBS J, 2019. **286**(6): p. 1154-1173.
30. Hunt, C.R., et al., *Histone modifications and DNA double-strand break repair after exposure to ionizing radiations.* Radiat Res, 2013. **179**(4): p. 383-92.
31. Goodarzi, A.A. and P.A. Jeggo, *The heterochromatic barrier to DNA double strand break repair: how to get the entry visa.* Int J Mol Sci, 2012. **13**(9): p. 11844-60.
32. Wright, D.E., C.Y. Wang, and C.F. Kao, *Histone ubiquitylation and chromatin dynamics.* Front Biosci (Landmark Ed), 2012. **17**: p. 1051-78.
33. Trujillo, K.M. and M.A. Osley, *A role for H2B ubiquitylation in DNA replication.* Mol Cell, 2012. **48**(5): p. 734-46.
34. Meas, R. and P. Mao, *Histone ubiquitylation and its roles in transcription and DNA damage response.* DNA Repair (Amst), 2015. **36**: p. 36-42.
35. Spannhoff, A., W. Sippl, and M. Jung, *Cancer treatment of the future: inhibitors of histone methyltransferases.* Int J Biochem Cell Biol, 2009. **41**(1): p. 4-11.
36. Kirmizis, A., et al., *Arginine methylation at histone H3R2 controls deposition of H3K4 trimethylation.* Nature, 2007. **449**(7164): p. 928-32.

37. Faucher, D. and R.J. Wellinger, *Methylated H3K4, a transcription-associated histone modification, is involved in the DNA damage response pathway.* PLoS Genet, 2010. **6**(8).
38. Klose, R.J., et al., *Demethylation of histone H3K36 and H3K9 by Rph1: a vestige of an H3K9 methylation system in Saccharomyces cerevisiae?* Mol Cell Biol, 2007. **27**(11): p. 3951-61.
39. Nichol, J.N., et al., *H3K27 Methylation: A Focal Point of Epigenetic Deregulation in Cancer.* Adv Cancer Res, 2016. **131**: p. 59-95.
40. McDaniel, S.L., et al., *H3K36 Methylation Regulates Nutrient Stress Response in Saccharomyces cerevisiae by Enforcing Transcriptional Fidelity.* Cell Rep, 2017. **19**(11): p. 2371-2382.
41. Nguyen, A.T. and Y. Zhang, *The diverse functions of Dot1 and H3K79 methylation.* Genes Dev, 2011. **25**(13): p. 1345-58.
42. Steiner, W.W. and E.M. Steiner, *Fission yeast hotspot sequence motifs are also active in budding yeast.* PLoS One, 2012. **7**(12): p. e53090.
43. TD., P., *Meiotic recombination hot spots and cold spots.* Nat Rev Genet., 2001. **2**(5): p. 360-369.
44. Martin-Castellanos, C., K.R. Fowler, and G.R. Smith, *Making chromosomes hot for breakage.* Cell Cycle, 2013. **12**(9): p. 1327-8.
45. Lam, I., N. Mohibullah, and S. Keeney, *Sequencing Spo11 Oligonucleotides for Mapping Meiotic DNA Double-Strand Breaks in Yeast.* Methods Mol Biol, 2017. **1471**: p. 51-98.
46. Murakami, H. and S. Keeney, *Regulating the formation of DNA double-strand breaks in meiosis.* Genes Dev, 2008. **22**(3): p. 286-92.
47. Johnson, D., et al., *Concerted cutting by Spo11 illuminates meiotic DNA break mechanics.* Nature, 2021. **594**(7864): p. 572-576.
48. Li, J., G.W. Hooker, and G.S. Roeder, *Saccharomyces cerevisiae Mer2, Mei4 and Rec114 form a complex required for meiotic double-strand break formation.* Genetics, 2006. **173**(4): p. 1969-81.
49. Panizza, S., et al., *Spo11-accessory proteins link double-strand break sites to the chromosome axis in early meiotic recombination.* Cell, 2011. **146**(3): p. 372-83.
50. Sasanuma, H., et al., *Cdc7-dependent phosphorylation of Mer2 facilitates initiation of yeast meiotic recombination.* Genes Dev, 2008. **22**(3): p. 398-410.
51. Claeys Bouuaert, C., et al., *DNA-driven condensation assembles the meiotic DNA break machinery.* Nature, 2021. **592**(7852): p. 144-149.
52. Maleki, S., et al., *Interactions between Mei4, Rec114, and other proteins required for meiotic DNA double-strand break formation in Saccharomyces cerevisiae.* Chromosoma, 2007. **116**(5): p. 471-86.
53. Li, J., G.W. Hooker, and G.S. Roeder, *Saccharomyces cerevisiae Mer2, Mei4 and Rec114 Form a Complex Required for Meiotic Double-Strand Break Formation.* Genetics, 2006. **173**(4): p. 1969-1981.
54. Gobbini, E., et al., *Functions and regulation of the MRX complex at DNA double-strand breaks.* Microb Cell, 2016. **3**(8): p. 329-337.

55. Ball, L.G., et al., *The Mre11-Rad50-Xrs2 complex is required for yeast DNA postreplication repair.* PLoS One, 2014. **9**(10): p. e109292.
56. Nakai, W., et al., *Chromosome integrity at a double-strand break requires exonuclease 1 and MRX.* DNA Repair (Amst), 2011. **10**(1): p. 102-10.
57. Jaehning, J.A., *The Paf1 complex: platform or player in RNA polymerase II transcription?* Biochim Biophys Acta, 2010. **1799**(5-6): p. 379-88.
58. Gothwal, S.K., et al., *The Double-Strand Break Landscape of Meiotic Chromosomes Is Shaped by the Paf1 Transcription Elongation Complex in Saccharomyces cerevisiae.* Genetics, 2016. **202**(2): p. 497-512.
59. Warner, M.H., K.L. Roinick, and K.M. Arndt, *Rtf1 is a multifunctional component of the Paf1 complex that regulates gene expression by directing cotranscriptional histone modification.* Mol Cell Biol, 2007. **27**(17): p. 6103-15.
60. Tomson, B.N., et al., *Identification of a role for histone H2B ubiquitylation in noncoding RNA 3'-end formation through mutational analysis of Rtf1 in Saccharomyces cerevisiae.* Genetics, 2011. **188**(2): p. 273-89.
61. Piro, A.S., et al., *Small region of Rtf1 protein can substitute for complete Paf1 complex in facilitating global histone H2B ubiquitylation in yeast.* Proc Natl Acad Sci U S A, 2012. **109**(27): p. 10837-42.
62. Van Oss, S.B., et al., *The Histone Modification Domain of Paf1 Complex Subunit Rtf1 Directly Stimulates H2B Ubiquitylation through an Interaction with Rad6.* Mol Cell, 2016. **64**(4): p. 815-825.
63. Amrich, C.G., et al., *Cdc73 subunit of Paf1 complex contains C-terminal Ras-like domain that promotes association of Paf1 complex with chromatin.* J Biol Chem, 2012. **287**(14): p. 10863-75.
64. Shilatifard, A., *The COMPASS family of histone H3K4 methylases: mechanisms of regulation in development and disease pathogenesis.* Annu Rev Biochem, 2012. **81**: p. 65-95.
65. Williamson K, S.V., et al. , *Catalytic and functional roles of conserved amino acids in the SET domain of the S. cerevisiae lysine methyltransferase Set1.* PLoS One, 2013. **8**(3): p. e57974.
66. Sommermeyer, V., et al., *Spp1, a member of the Set1 Complex, promotes meiotic DSB formation in promoters by tethering histone H3K4 methylation sites to chromosome axes.* Mol Cell, 2013. **49**(1): p. 43-54.
67. Acquaviva, L., et al., *The COMPASS subunit Spp1 links histone methylation to initiation of meiotic recombination.* Science, 2013. **339**(6116): p. 215-8.
68. de Massy, B., *Spp1 links sites of meiotic DNA double-strand breaks to chromosome axes.* Mol Cell, 2013. **49**(1): p. 3-5.
69. S.Keeney, M.J.N., *Initiation of meiotic recombination by formation of DNA double-strand breaks: mechanism and regulation.* Biochem Soc Trans., 2006. **34**(Pt4): p. 523-5.
70. Borner, G.V. and R.S. Cha, *Analysis of Yeast Sporulation Efficiency, Spore Viability, and Meiotic Recombination on Solid Medium.* Cold Spring Harb Protoc, 2015. **2015**(11): p. 1003-8.
71. Schwacha, A. and N. Kleckner, *Interhomolog bias during meiotic recombination: meiotic*

functions promote a highly differentiated interhomolog-only pathway. Cell, 1997. **90**(6): p. 1123-35.

72. Kim, K.P., et al., *Sister cohesion and structural axis components mediate homolog bias of meiotic recombination.* Cell, 2010. **143**(6): p. 924-37.
73. S.K. Gothwal, et al., *The Double-Strand Break Landscape of Meiotic Chromosomes Is Shaped by the Paf1 Transcription Elongation Complex in Saccharomyces cerevisiae.* Genetics, 2016. **202**(2): p. 497-512.
74. Taylor, M.R.G., et al., *Rad51 Paralogs Remodel Pre-synaptic Rad51 Filaments to Stimulate Homologous Recombination.* Cell, 2015. **162**(2): p. 271-286.
75. Carballo, J.A., et al., *Budding yeast ATM/ATR control meiotic double-strand break (DSB) levels by down-regulating Rec114, an essential component of the DSB-machinery.* PLoS Genet, 2013. **9**(6): p. e1003545.
76. Malone, R.E., et al., *The signal from the initiation of meiotic recombination to the first division of meiosis.* Eukaryot Cell, 2004. **3**(3): p. 598-609.
77. Nag, D.K., et al., *Both conserved and non-conserved regions of Spo11 are essential for meiotic recombination initiation in yeast.* Mol Genet Genomics, 2006. **276**(4): p. 313-21.
78. Sasanuma, H., et al., *Meiotic association between Spo11 regulated by Rec102, Rec104 and Rec114.* Nucleic Acids Res, 2007. **35**(4): p. 1119-33.
79. Kugou, K., et al., *Rec8 guides canonical Spo11 distribution along yeast meiotic chromosomes.* Mol Biol Cell, 2009. **20**(13): p. 3064-76.
80. Bishop, D.K., et al., *DMC1: a meiosis-specific yeast homolog of E. coli recA required for recombination, synaptonemal complex formation, and cell cycle progression.* Cell, 1992. **69**(3): p. 439-56.
81. Lee, J.S., et al., *Histone crosstalk between H2B monoubiquitination and H3 methylation mediated by COMPASS.* Cell, 2007. **131**(6): p. 1084-96.
82. Worden, E.J. and C. Wolberger, *Activation and regulation of H2B-Ubiquitin-dependent histone methyltransferases.* Curr Opin Struct Biol, 2019. **59**: p. 98-106.
83. Rumpf, C., et al., *Casein kinase 1 is required for efficient removal of Rec8 during meiosis I.* Cell Cycle, 2010. **9**(13): p. 2657-62.
84. Wood, A., et al., *The Paf1 complex is essential for histone monoubiquitination by the Rad6-Bre1 complex, which signals for histone methylation by COMPASS and Dot1p.* J Biol Chem, 2003. **278**(37): p. 34739-42.
85. Adam, C., et al., *The PHD finger protein Spp1 has distinct functions in the Set1 and the meiotic DSB formation complexes.* PLoS Genet, 2018. **14**(2): p. e1007223.
86. Acquaviva, L., et al., *Spp1 at the crossroads of H3K4me3 regulation and meiotic recombination.* Epigenetics, 2013. **8**(4): p. 355-360.
87. Latham, J.A., et al., *Chromatin signaling to kinetochores: transregulation of Dam1 methylation by histone H2B ubiquitination.* Cell, 2011. **146**(5): p. 709-19.